Modeling Local Aerosol Surface Environments: Clustering of Organic Acids, Water, and Ions

Georg Baadsgaard Trolle, Jakub Kubečka, and Jonas Elm*

Department of Chemistry, Aarhus University, Langelandsgade 140, 8000 Aarhus C, Denmark

E-mail: jelm@chem.au.dk

Phone: +45 28938085

Abstract

Pyruvic acid is an omnipresent compound in nature and is found both in the gas-phase and in the particle-phase of the atmosphere as well as in aqueous solution in the hydrosphere. Despite much literature on the photochemical degradation and stability of pyruvic acid in different chemical environments, the study of simultaneous interactions between gas-phase pyruvic acid or similar carboxylic acids with water and ions is not well-understood. Here, we present a study of micro-hydrated molecular clusters containing pyruvic acid and the structural analogous caboxylic acids lactic acid, propionic acid, and 2,2-dihydroxypropanoic acid by probing geometries, binding free energies, hydrate distributions, as well as their IR absorption spectra. We performed a meticulous configurational sampling protocol for the various hydrated clusters ranging from low level of theory to high level of theory to identify the lowest free energy structure. We find that cluster geometries and especially their water structure are highly sensitive to the presence and character of ions. We show that the hydration of the studied organic acids is thermodynamically unfavorable in the gas-phase and ions are necessary for mediating interactions between organic acids and water thus stabilizing the clusters. Finally, we find a clear correlation between decreasing pyruvic acid carboxylic O–H stretching frequencies, increasing intensity when adding more water to the clusters, and a correlation between increasing red-shifting of the O–H frequencies upon addition of ions to the clusters. The observations done in this study could pave the way to unravel the mechanisms behind the transitioning of organic acids from the gas-phase to the particle phase.

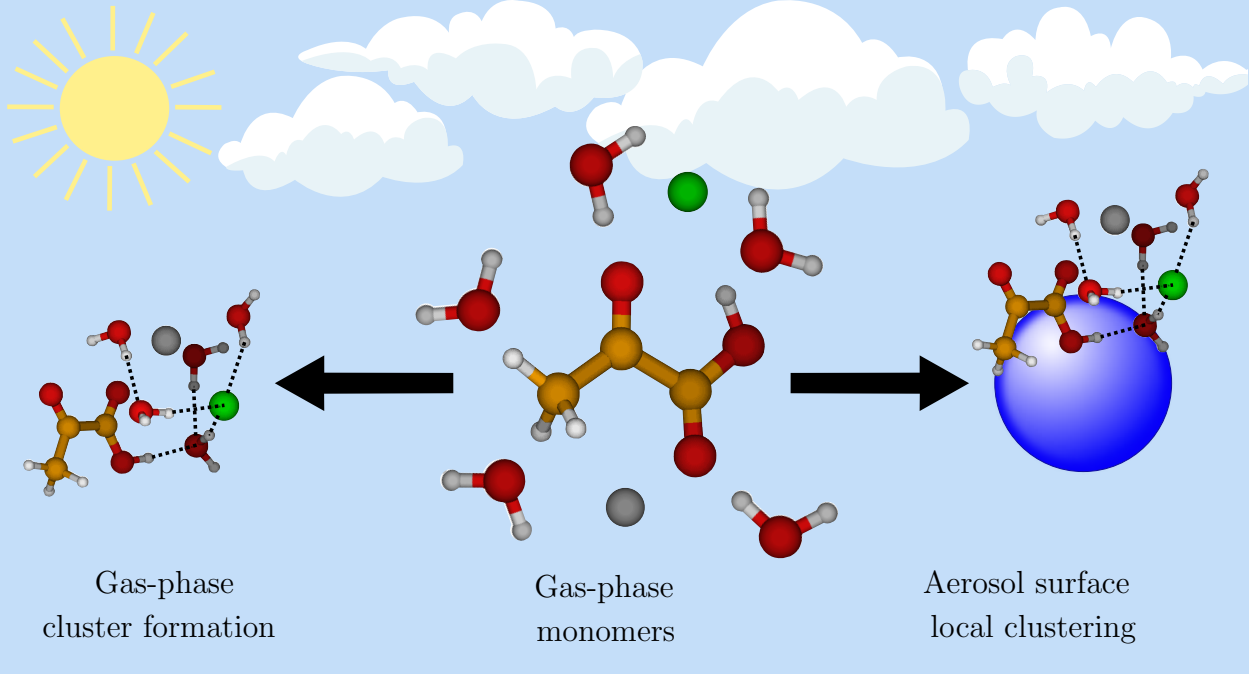

1 Introduction

The small organic acid, pyruvic acid (PA), and its conjugate base, the pyruvate ion (PA^-), are common chemical constituents of aerosols, fogs, clouds as well as seawater.[1,2] PA is ubiquitous in the atmosphere and emitted from both biogenic and anthropogenic sources and has been detected as a major component of secondary organic aerosols (SOA) at many geographic locations.[3,4] These include the urban atmospheres of Japan,[5] China,[6–8] and Mongolia[9] but PA has also been detected in remote aerosols at mountaintops in China,[3] tropic Indian aerosols,[10] marine aerosols,[11–13] arctic aerosols,[14] and even in biomass burning aerosols in Brazil.[15] The particle-phase concentration of PA has been observed to possess a large spatiotemporal variability with average particle-phase concentrations measured as high as 49.7 ng m^{-3} in SOA of the urban atmosphere of Tokyo, Japan and as low as 0.03 ng m^{-3} in marine aerosols over the Southern Ocean.[5,12] Furthermore, particle-phase concentrations of PA are observed to fluctuate significantly depending on season.[4,5]

In the aqueous phase, PA has been subjected to many photochemical investigations and has been reported to produce acetoin, lactic acid, and acetic acid and possibly also contribute to SOA mass through an oligomerization process, which goes via the parapyruvic acid dimer.[16–20] Furthermore, PA has been found to exist as a mixture of the keto form and its hydrate, the geminal diol 2,2-dihydroxypropanoic acid (termed diol in this study).[20,21] Hence, PA interconverts between the diol, the conjugate base of the diol, and the conjugate base of PA, PA^-, in a cyclic manner.[20] The ratio of abundances of the keto form and the diol has previously been reported to be 65% diol and 35% keto in aqueous solution, at 298 K and neutral pH.[16,20,22] Furthermore, the pK_a of PA in its keto form in aqueous solution and at 298 K is determined to be 2.18 while for the diol, it is determined to be 3.6.[20] In perspective, aerosols are usually acidic with a median pH of 2.5, which implies that PA in its keto form is the most favored in aerosols at normal ambient conditions.[23] In addition to the pure aqueous-phase studies of PA, there has also been conducted several photochemical experiments of PA in e.g. multiphase environments and at air-water interfaces in order to probe the dynamic

equilibrium between PA in the aqueous phase and PA in the gas-phase.[24,25]

PA has also been studied extensively in the gas-phase.[2,26–30] The gas-phase mixing ratio of PA has mainly been measured in the range 10-100 pptv but has been detected as high as 400 pptv in the Amazonas region of Brazil and in the southern US.[2,27,30] The atmospheric sources of PA in the troposphere are manifold and the routes to its formation goes mainly through gas-phase photolysis of small organic precursors. This includes the photo-oxidation of isoprene via the ozonolysis of methyl vinyl ketone,[31–33] the photolysis of methylglyoxal,[34] the reactions of peroxy radicals formed in the oxidation of propane, acetone, and hydroxyacetone,[35,36] and in the photo-oxidation of aromatic compounds in the presence of NO_x.[37,38] The atmospheric sinks of PA, on the other hand, are generally four-fold: i) By rapid gas-phase photolysis induced by actinic radiation;[39] ii) by slow gas-phase reaction with OH radicals;[2] by wet and dry deposition, and iv) by partitioning into the aerosol particle-phase.[16–18,40–43] The atmospheric fate of PA via photolysis proceeds primarily via an exothermic decarboxylation, which involves a five-membered transition state that decomposes into CO_2 and methylhydroxycarbene with the latter rapidly rearranging to acetaldehyde.[2,30] The gas-phase lifetime of PA with respect to the photolysis channel is a few hours according to previous experimental studies.[44,45] Conversely, the gas-phase lifetime of PA against the OH channel is significantly longer at about three months.[46] The atmospheric fate of PA via the dry and wet deposition mechanisms as well as by the partitioning into the aerosol-phase are particularly pronounced at high relative humidity due to the high solubility of PA in water and can thus contribute to the formation of SOA.[16–18,40–43]

While the gas-phase and aqueous phase chemistry of PA has been extensively studied, the transition between the two has not yet been investigated in detail. The uptake of PA onto aerosol particles must occur via the interfacial surface layer. As a first approximation the local environment of the interaction between the gas phase PA and the surface can be viewed as a small cluster of molecules consisting of water and ions. Despite previous studies on the PA monohydrate cluster, the diol in the liquid phase[21] and the PA clusters with one

to four water molecules,[47] there has, to the best of our knowledge, not been reported any studies on how PA or similar carboxylic acids simultaneously interact with water molecules and ions.

In this study, we investigate clusters of PA and its structurally similar analogs, lactic acid (LA), propionic acid (ProA), and 2,2-dihydroxypropionic acid (diol), by probing the geometries, computing cluster binding free energies, hydrate distributions, and IR absorption spectra. We specifically look at the intermolecular interactions between the organic acids, water and ions (Na^+, Cl^- and a NaCl pair). By viewing such clusters as a representation of the local aerosol surface environment, our aim is to elucidate how such small organic acids interact with the surface and enters the particle.

2 Computational Details

Initial configurational sampling was performed with ABCluster program version 2.0, using a CHARMM force field.[48,49] Subsequent single-point energies, geometries, and configurational sampling were calculated employing the GFN1-xTB method[50] in the xtb software versions 6.4.0 and 6.4.1.[51] Gaussian 16 version B.01 was utilized for the DFT geometry optimizations and vibrational frequency calculations at the ωB97X-D/6-31++G(d,p) level of theory.[52] ORCA version 5.0.4 was employed for calculating high level single-point energies using the DLPNO-CCSD(T_0)/aug-cc-pVTZ level.[53] The DLPNO-CCSD(T_0)/aug-cc-pVTZ//ωB97X-D/6-31++G(d,p) level of theory has been used extensively in the literature[54–61] for studying the binding energetics of atmospheric molecular clusters and the choice is corroborated by additional benchmarking of the PA structures and interaction energies, carried out in this work (see Supporting Information). The above software was used as third-party programs implemented in the JKCS program, which fully automate the cluster configurational sampling.[62]

2.1 Cluster Systems

We studied the $(PA)_1(w)_{0-5}$, $(LA)_1(w)_{0-5}$, $(ProA)_1(w)_{0-5}$, $(diol)_1(w)_{0-5}$, $(PA)_1(Na^+)_{0-1}(Cl^-)_{0-1}(w)_{0-5}$, $(PA^-)_1(w)_{0-5}$ and the $(PA^-)_1(Na^+)_1(Cl^-)_{0-1}(w)_{0-5}$ cluster systems. Figure 1**B** below presents the four different conformers of PA.[63] The PA conformers are conventionally assigned conformational abbreviations according to the cis-trans nomenclature, with the first letter denoting the geometric relationship between the two carbonyl groups and the second letter denoting the geometric relationship between the α-carbonyl group and the carboxylic acid proton.[63] Blair et al. calculated the relative zero-point vibrational corrected electronic energies of the four PA conformers to be 0.00 kcal/mol for the **Tc** conformer, 2.68 kcal/mol for the **Tt** conformer, 4.36 kcal/mol for the **Ct** conformer, and 10.31 kcal/mol for the **Cc** conformer at 298 K and at the ωB97X-D/aug-cc-pVTZ level of theory.[63]

In addition to the conformers of PA, Figure 1**A** and Figure 1**D** provide a general overview of the clusters and monomers probed in this study and Figure 1**C** provides the conformers of LA.

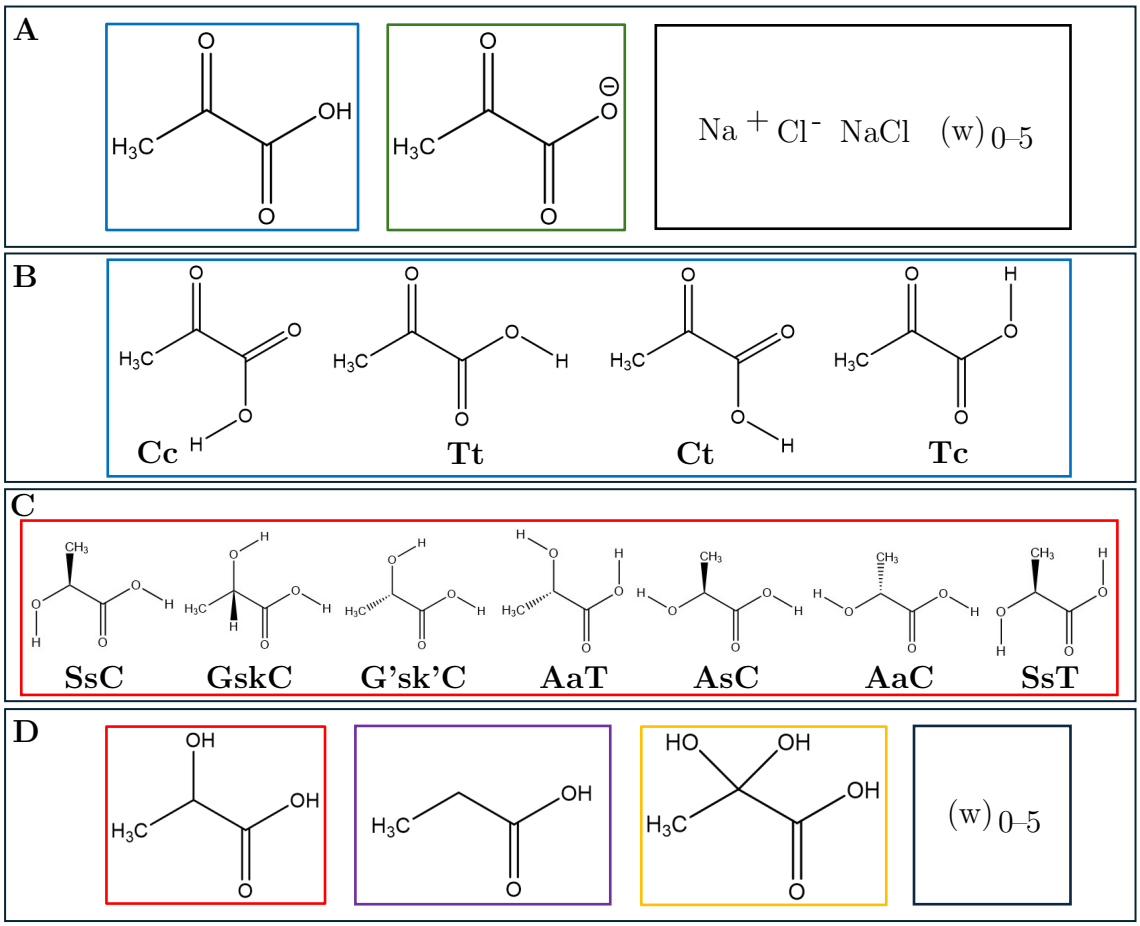

Figure 1: Overview of the various organic acids probed in this study. **A** PA (blue frame), PA^- (green frame), and ions with water (w) (black frame); **B** the four conformers of PA termed according to the cis–trans nomenclature;[63] **C** The seven conformers of LA assigned conformational abbreviations in conformity with the nomenclature of Borba et al.;[64] **D** LA (red frame), ProA (purple frame), diol (yellow frame), and water (black frame). Note that there are two conformers of ProA corresponding to an eclipsed and a staggered conformer, which are not represented here. Note also that there are four conformers of the diol but as these are equivalent to the conformers of PA, they are omitted for clarity.

2.2 Configurational Sampling

We employed a well-established, extensive configurational sampling (CS) protocol to obtain the cluster structures. The ABCluster input files for PA, LA, ProA, and the diol were generated with topgen.[65] Hirshfeld population analysis was calculated at the MP2/6-31++G(d,p) level of theory.[66] We used the Charge Model 5 (CM5), which has a reduced basis set sensitivity and geometry dependency.[67] The overall configurational sampling workflow can be described as follows:

$$\text{ABCluster} \xrightarrow[\text{sort}\Delta E]{2000} \text{GFN1-xTB}^{\text{OPT}} \xrightarrow[\text{filtering}]{\Delta(E,dip,R_g)} \text{DFT}^{\text{OPT/FREQ}} \xrightarrow[\text{sort}\Delta G]{5} \text{DLPNO-CCSD(T}_0\text{)}^{\text{SP}}$$

The ABCluster search was performed based on the parameters recommended by Kubečka et al., with a population of $SN = 300$ times the number of molecules in the cluster, number of generations $g_{\max} = 200$, and a maximal structure lifetime of $sc = 4$ generations for all cluster sizes.[68] All protonation states of water (H_2O, H_3O^+, and OH^-) leading to electrical neutral clusters and all conformers of PA, LA, ProA, and the diol were employed in the ABCluster search. The overall number of local minima saved for subsequent GFN1-xTB calculations was 2000 ($lm = 2000/NS$, where NS refers to the total number of simulations) and were sorted with respect to electronic energy.

The selected structures were pre-optimized at the GFN1-xTB level.[50] After the pre-optimization, a filtering maneuver was performed with respect to the collective variables: Electronic energy (0.001 Ha cut-off), radius of gyration (0.01 Å cut-off), and electric dipole moment (0.1 D cut-off) to identify unique configurations.

After filtering, full geometry optimization and vibrational frequency calculations were performed at ωB97X-D/6-31++G(d,p) level of theory.[52] Structures where the lowest vibrational frequencies were negative and structures, which did not converge were resubmitted for further optimization. After all DFT calculations were finished, the quasi-harmonic approx-

imation were applied using a frequency cut-off at 100 cm^{-1}.[69,70] All frequencies below this cut-off are treated as free rotations when calculating the entropy. Finally, single-point electronic energies were calculated with the DLPNO-CCSD(T_0) method on the five structures lowest in Gibbs free energy.[71,72] For these calculations, the RI-JK approximation with the aug-cc-pVTZbasis set, and with an auxiliary basis set for the Coulomb and exchange parts was applied together with the TightSCF convergence criterion.

2.2.1 Calculations of Binding Free Energies

The binding free energy (ΔG_{bind}) of the clusters is defined as:

$$\Delta G_{\text{bind}} = G_{\text{cluster}} - (G_{\text{monomer}} + n \cdot G_{\text{water}} + m \cdot G_{\text{ions/salt}}), \quad (1)$$

where G_{monomer} corresponds to the Gibbs free energy of the organic acid monomer, G_{water} corresponds to the Gibbs free energy of a water molecule, $G_{\text{ions/salt}}$ corresponds to the Gibbs free energy of the Na^+ or Cl^- ion or the NaCl pair, and n and m correspond to the number of water molecules and the number of ions in the cluster, respectively. We calculate the Gibbs free energy for each cluster component as a combination of a high-level electronic contribution and a DFT thermal free correction:

$$G^{\text{DLPNO-CCSD(T)//}\omega\text{B97X-D}} = E_{\text{corr}}^{\text{DLPNO-CCSD(T)}} + G_{\text{thermal}}^{\omega\text{B97X-D}} \quad (2)$$

Here the free energies are computed at 298.15 K and 1 atm. Free energies at other temperatures are calculated based on the assumption that the enthalpy and entropy does not change significantly when changing the temperature.

For the hydration distributions presented in this study, we apply the following equation obtained from statistical mechanics and classical nucleation theory:

$$\frac{c_n}{\sum_i c_i} = \frac{\left(\frac{p_{\mathrm{w}}}{p_{\mathrm{ref}}}\right)^n \exp(-\frac{\Delta G_{\mathrm{bind},n}}{k_{\mathrm{B}}T})}{\sum_i \left(\frac{p_{\mathrm{w}}}{p_{\mathrm{ref}}}\right)^i \exp(-\frac{\Delta G_{\mathrm{bind},i}}{k_{\mathrm{B}}T})} \tag{3}$$

where c_n is the concentration (or probability) of a cluster of size n, c_i is the concentration (or probability) of a cluster component i, p_w and p_{ref} are the partial pressures water and the equilibrium saturation vapor pressure of water, respectively, $\Delta G_{\mathrm{bind,n}}$ is the binding free energy associated with forming a cluster of size n, $\Delta G_{\mathrm{bind,i}}$ is the binding free energy associated with the cluster component, i, k_B is the Boltzmann constant, and T is the temperature.

2.3 IR Absorptions of Pyruvic Acid Clusters

Multiple experimental studies have been reported on the H-shift for the intramolecular hydrogen bond between the carboxylic O–H bond and the α-carbonyl group of PA.[28,29] Thus, vibrational spectroscopy has been an important tool in distinguishing between the various conformers of PA.

In order to computationally probe the hydrogen bond shift of the PA carboxylic O–H bond in the clusters, we calculated IR spectra of the various PA-containing clusters. GaussView version 6.0.16[73] was employed for visually inspecting the vibrational normal modes of the clusters and identifying the relevant carboxylic O–H stretching vibration. The discrete vibrational modes for the global minimum structure of each cluster corresponding to the carboxylic O–H stretching vibration were then collected and presented as an IR spectrum.

3 Results and Discussion

3.1 Cluster Geometries

3.1.1 The Reference Systems

To test our configurational sampling methodology, we initially studied the simple $(w)_{0-5}$, $(Na^+)_1(w)_{0-5}$, and $(Cl^-)_{0-1}(w)_{0-5}$ cluster systems. We obtained the cluster structures shown in Figure 2. The clusters are calculated at the DLPNO-CCSD(T_0)/aug-cc-pVTZ//ωB97X-D/6-31++G(d,p) level of theory, at 298.15 K and 1 atm using the quasi-harmonic approximation.

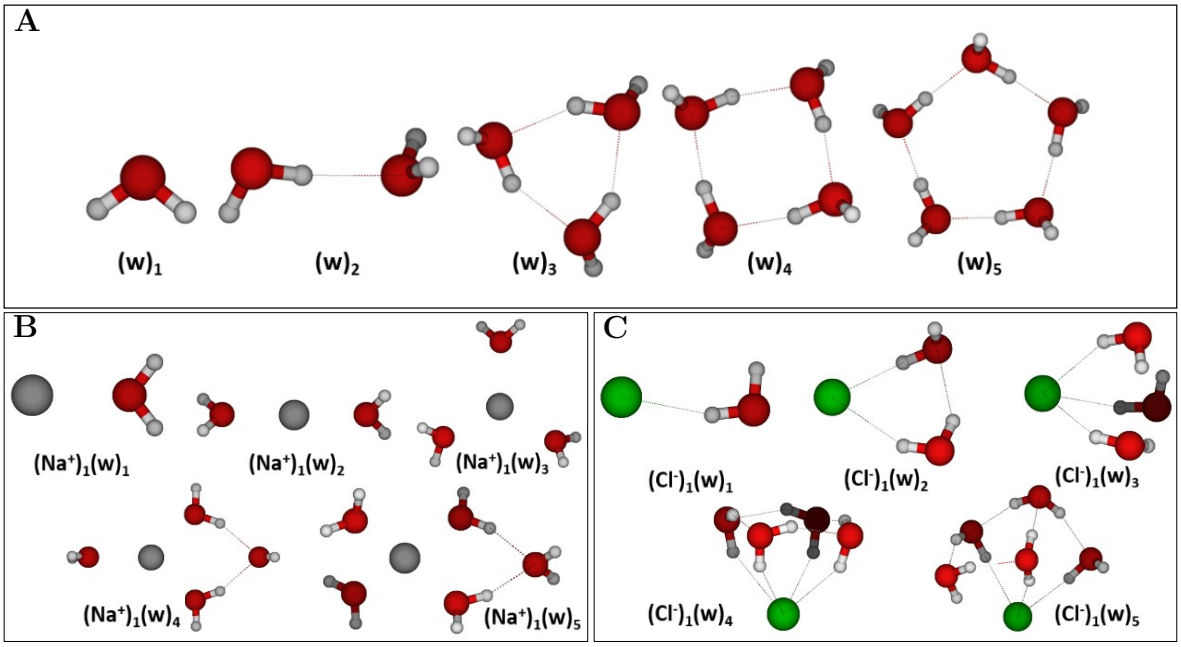

Figure 2: The lowest free energy clusters of water (w) and microhydrated Na^+ and Cl^- ions: **A** $(w)_{1-5}$; **B** $(Na^+)_1(w)_{1-5}$; **C** $(Cl^-)_1(w)_{1-5}$. Calculated at the DLPNO-CCSD(T_0)/aug-cc-pVTZ//ωB97X-D/6-31++G(d,p) level of theory, at 298.15 K and 1 atm using the quasi-harmonic approximation. Hydrogen atoms are white, oxygen red, sodium gray, and chlorine green.

Multiple experimental studies have reported the gas-phase micro-hydration of the sodium ion[74–80] along with computational investigations.[81–101] In a similar manner the micro-hydration of the chloride ion has also been studied experimentally,[80,102,103] in addition to computational

investigations.[83,84,87,88,97,103–105] Generally, we see high similarity between our geometries obtained at the ωB97X-D/6-31++g(d,p) level of theory and literature geometries obtained at the MP2/aug-cc-pVDZ level of theory for the hydrated gas-phase clusters of a sodium ion[101] and a chloride ion.[97] In a similar manner our identified $(w)_{1-5}$ cluster geometries seen in Figure 2**A** follow the conventional structure of pure gas-phase water clusters reported in the literature.[106–108]

Figure 2**B** shows the $(Na^+)_1(w)_{1-5}$ cluster geometries. For $(Na^+)_1(w)_1$, we observe an ion-dipole interaction. For $(Na^+)_1(w)_2$, we wee a linear assembly of water molecules with the Na^+ center. For $(Na^+)_1(w)_3$, the cluster adopts a trigonal planar geometry of the waters surrounding the Na^+ center. For the $(Na^+)_1(w)_4$ cluster, a quasi-square planar geometry is seen, due to the additional water molecule (confirmed with literature geometries[88,91,101]) but is also reported to be able to adopt a tetrahedral geometry.[88,91,101] For $(Na^+)_1(w)_5$, four water molecules are interacting with Na^+ and one water resides at the periphery of the cluster, which corresponds to the most reported literature geometries even though square pyramidal geometries also occur.[88,91,101]

Figure 2**C** presents the $(Cl^-)_1(w)_{1-5}$ cluster geometries. For $(Cl^-)_1(w)_1$, we observe a polarization-enhanced hydrogen bond. For $(Cl^-)_1(w)_2$, we see a trigonal planar geometry of all components without an ionic center (in contrast to the $(Na^+)_1(w)_3$ cluster described above). For $(Cl^-)_1(w)_3$, the cluster adopts a trigonal pyramidal geometry around the central Cl^-. For the $(Cl^-)_1(w)_4$ cluster, a square pyramidal geometry around the central Cl^- is seen. For $(Cl^-)_1(w)_5$, a quasi-square pyramidal geometry around the central Cl^- is observed, which possess a slight deviation from the four-water planarity observed in the $(Cl^-)_1(w)_4$ cluster. In general, the $(Cl^-)_1(w)_{1-5}$ clusters are also in full agreement with literature geometries.[97,103,105]

Overall, Na^+ is generally observed to be encapsulated inside the clusters and solvated by the surrounding water molecules. In contrast the Cl^- ion is residing at the edge of the clusters.

3.1.2 The Hydration of Organic Acids

Using the outlined configurational sampling protocol we studied the $(PA)_1(w)_{0-5}$, $(LA)_1(w)_{0-5}$, $(ProA)_1(w)_{0-5}$, and $(diol)_1(w)_{0-5}$ cluster systems. Figure 3 presents the hydrated cluster geometries of PA (Figure 3**A**), LA (Figure 3**B**), ProA (Figure 3**C**), and the diol (Figure 3**D**). All calculations are performed at the DLPNO-CCSD(T_0)/aug-cc-pVTZ//ωB97X-D/6-31++G(d,p) level of theory, at 298.15 K and 1 atm.

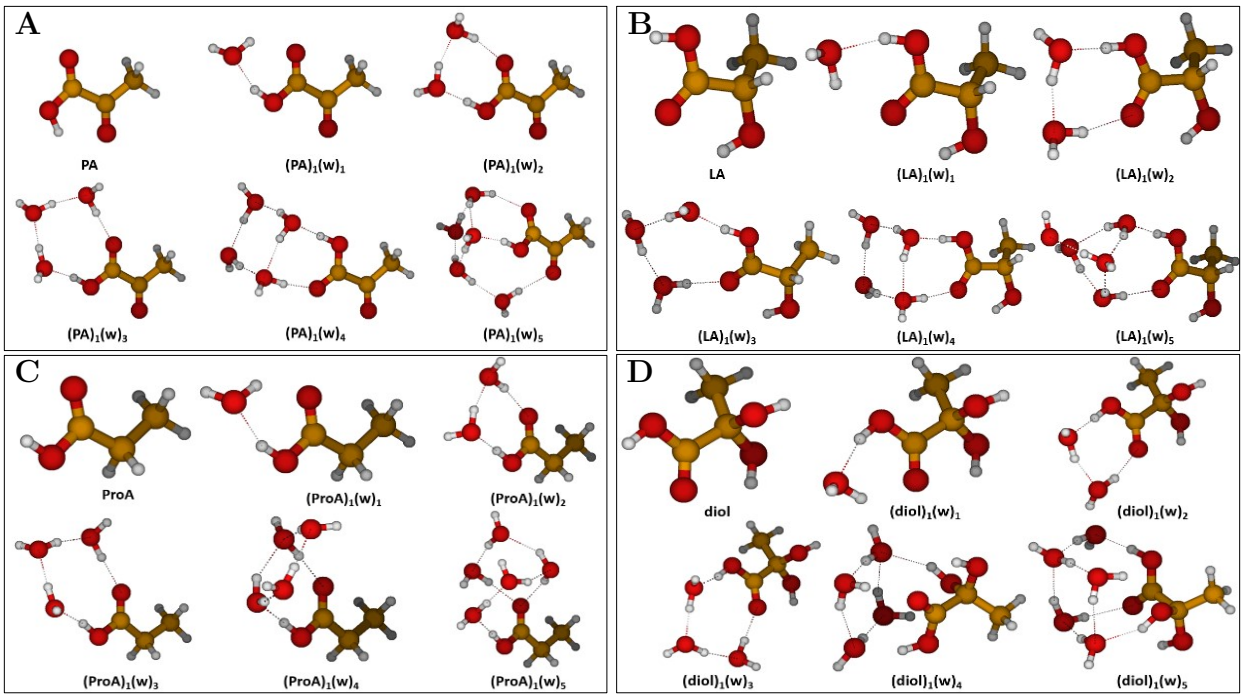

Figure 3: The lowest free energy clusters of PA, LA, ProA, and diol with up to five water (w) molecules: **A** $(PA)_1(w)_{0-5}$; **B** $(LA)_1(w)_{0-5}$; **C** $(ProA)_1(w)_{0-5}$; **D** $(diol)_1(w)_{0-5}$. Calculated at the DLPNO-CCSD(T_0)/aug-cc-pVTZ//ωB97X-D/6-31++G(d,p) level of theory, at 298.15 K and 1 atm using the quasi-harmonic approximation. Hydrogen atoms are white, carbon brown, and oxygen red.

In no cases do we observe a proton transfer from the organic acids to water. As seen in Figure 3**A**, the **Tc** conformer of PA was identified as the lowest free energy conformer, as expected. However, when hydrating the monomer, it takes the form of the **Tt** conformer within the $(PA)_1(w)_{1-3}$ and $(PA)_1(w)_5$ clusters. This can be ascribed to the PA monomer engaging in favorable hydrogen-bonding interactions with the surrounding water molecules

thus impeding intramolecular hydrogen bonding between the carboxylic O–H donor and the α-carbonyl acceptor. In the $(PA)_1(w)_4$ cluster, the **Ct** conformer of PA is observed instead but the configuration of the carboxylic acid moiety is retained as the **Ct** conformer is simply generated by a 180-degree rotation around the C–C bond of the two carbonyl groups of the **Tc** conformer. Generally, the water molecules are observed to reside at the carboxylic acid terminus of the PA monomer and the hydrogen bonding capacity of the carboxylic oxygens are observed to be saturated at the $(PA)_1(w)_4$ cluster, i.e., the fifth water molecule in the $(PA)_1(w)_5$ cluster engages in hydrogen bonding with the α-carbonyl group instead, thus serving as a water bridge to the adjacent four-water ensemble.

When comparing the PA clusters with literature, we find that the $(PA)_1(w)_1$ cluster is consistent with the cluster obtained by Petersen-Sonn et al.[47] at CAM-B3LYP/aug-cc-pVTZ level of theory and by Shemesh et al.[109] at MP2/cc-pVDZ level of theory. However, for the $(PA)_1(w)_{2-5}$ clusters we find slight discrepancies between our geometries and the literature geometries as the water structure here is much more diffuse compared to our well-centered and well-organized water structure. These geometric discrepancies could be ascribed to both differences in configurational sampling protocol and level of theory.

In case of the PA analogs in Figure 3**B-D**, we observe very similar geometrical patterns as for the PA clusters in Figure 3**A**. For the $(LA)_1(w)_{0-5}$ clusters, the SsC conformer of LA[64] is the lowest free energy conformer across all clusters due to the intramolecular hydrogen bond between the α-hydroxy group and the carboxylic carbonyl group as well as the minimization of steric repulsions induced by the methyl group as it protrudes away from the carboxylic acid plane of LA. For the $(ProA)_1(w)_{0-5}$ clusters, ProA takes the planar and entirely staggered conformer over the bent conformer across all clusters. For the $(diol)_1(w)_{0-5}$ clusters, the **Ct** conformer dominates across all clusters due to the intramolecular hydrogen bond between the carboxylic carbonyl group and one of the α-hydroxy groups while the other α-hydroxy group and the methyl group protrude away from the main carboxylic acid plane of the diol.

Generally for all organic acid clusters containing four water molecules in Figure 3, we

observe a conservation of the water structure with respect to the pure water cluster containing four water molecules presented in Figure 2**A** above.

3.1.3 The Pyruvic Acid-Containing Clusters

We studied the $(PA)_1(Na^+)_{0-1}(Cl^-)_{0-1}(w)_{0-5}$ cluster systems to investigate the influence of ions on the PA-containing clusters. Figure 4 shows clusters with sodium ion, with chloride ion, and with both ions simultaneously.

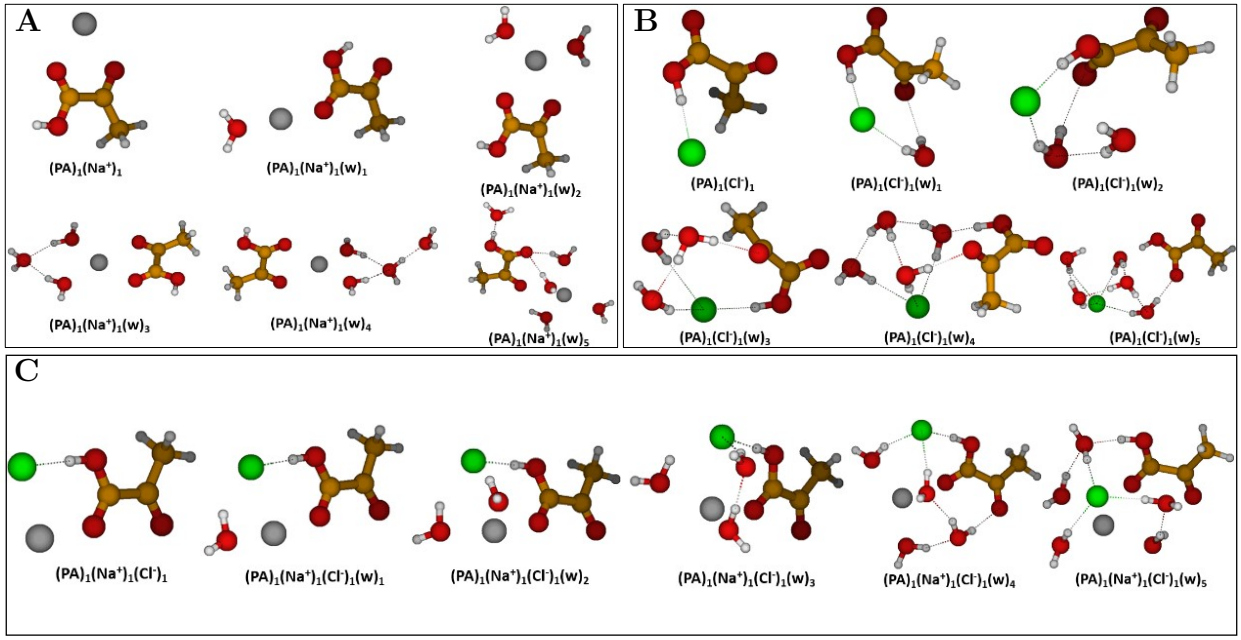

Figure 4: The lowest free energy clusters of PA, Na^+, and Cl^- with up to five water (w) molecules. **A** $(PA)_1(Na^+)_1(w)_{0-5}$; **B** $(PA)_1(Cl^-)_1(w)_{0-5}$; **C** $(PA)_1(Na^+)_1(Cl^-)_1(w)_{0-5}$. Calculated at the DLPNO-CCSD(T_0)/aug-cc-pVTZ//ωB97X-D/6-31++G(d,p) level of theory, at 298.15 K and 1 atm using the quasi-harmonic approximation. Hydrogen atoms are white, carbon brown, oxygen red, and sodium gray, and chlorine green.

Generally, we observe no proton transfers in these clusters. For the $(PA)_1(Na^+)_{1-5}$ clusters in Figure 4**A**, PA prefers the **Ct** conformer. This can be ascribed to the bifurcated ion-dipole interactions between the adjacent carbonyl oxygens of PA and Na^+. The water molecules are generally observed to reside on the other side of Na^+ for the $(PA)_1(Na^+)_1(w)_{1-4}$ clusters thus building up a hydrogen-bonded water network solely interacting with the Na^+ ion. However,

for the $(PA)_1(Na^+)_1(w)_5$ cluster, we observe that the Na^+ ion is "solvated" by the water molecules, thus residing more remotely from the PA monomer.

Upon visual inspection of the $(PA)_1(Cl^-)_1(w)_{0-5}$ in Figure 4**B**, we observe a much broader variation in the preferred PA conformer across the hydrated clusters. PA prefers the **Cc** conformer in the $(PA)_1(Cl^-)_1$ dimer cluster. For the $(PA)_1(Cl^-)_1(w)_1$ cluster, the C–C bond rotation between the carbonyl groups of PA has occurred and the **Tc** conformer is now preferred. The relative geometry between the carboxylic O–H and the α-carbonyl group is not completely planar as it is in the ordinary **Tc** conformer, which can be ascribed to better steric access of Cl^- and the water molecule to engage in hydrogen bond interactions with the carboxylic O–H and the α-carbonyl group, respectively. In the $(PA)_1(Cl^-)_1(w)_2$ cluster, the C–C bond has rotated further, and thus PA adopts the **Ct** form thereby interacting with Cl^- through the carboxylic O–H and water through the carboxylic carbonyl group. For the $(PA)_1(Cl^-)_1(w)_{3-4}$ clusters, the C–C bond is rotated such that PA is effectively a superposition between the **Tc** and **Cc** conformers. Finally, in the $(PA)_1(Cl^-)_1(w)_5$ cluster, we observe the **Tt** conformer to be the preferred PA conformer. Here, we observe the water molecules to have formed a hydrogen bonding network encapsulating the Cl^- thus screening Cl^- from forming hydrogen bonds with the carboxylic O–H.

For the $(PA)_1(Na^+)_1(Cl^-)_1(w)_{0-5}$ clusters in Figure 4**C**, the **Ct** conformer is the preferred form across all clusters. The Cl^- ion engages in hydrogen bonding with the carboxylic O–H in $(PA)_1(Na^+)_1(Cl^-)_1(w)_{0-4}$, while it is encapsulated by water and screened from interacting in $(PA)_1(Na^+)_1(Cl^-)_1(w)_5$. Generally across the clusters, we see that the Na^+ ion and the Cl^- ion reside in close proximity to each other and form an ion pair, which interacts with the carboxylic O–H group and the carbonyl group of the PA monomer. However, these interactions are mitigated when more water is added to the clusters. We also observe a general ion solvation point when reaching five waters in the various hydrated clusters where the ion is encapsulated and isolated from the PA monomer by the nascent water hydrogen bonding network.

Overall, introducing ions into the system, highly perturbs the cluster geometries.

3.1.4 The Pyruvate-Containing Clusters

To study the conjugate base of PA, the pyruvate ion, we investigated the $(PA^-)_1(w)_{0-5}$ and $(PA^-)_1(Na^+)_1(Cl^-)_{0-1}(w)_{0-5}$ cluster systems. Figure 5 presents the structures of the studied systems, calculated at the DLPNO-CCSD(T_0)/aug-cc-pVTZ//ωB97X-D/6-31++G(d,p) level of theory, at 298.15 K and 1 atm using the quasi-harmonic approximation.

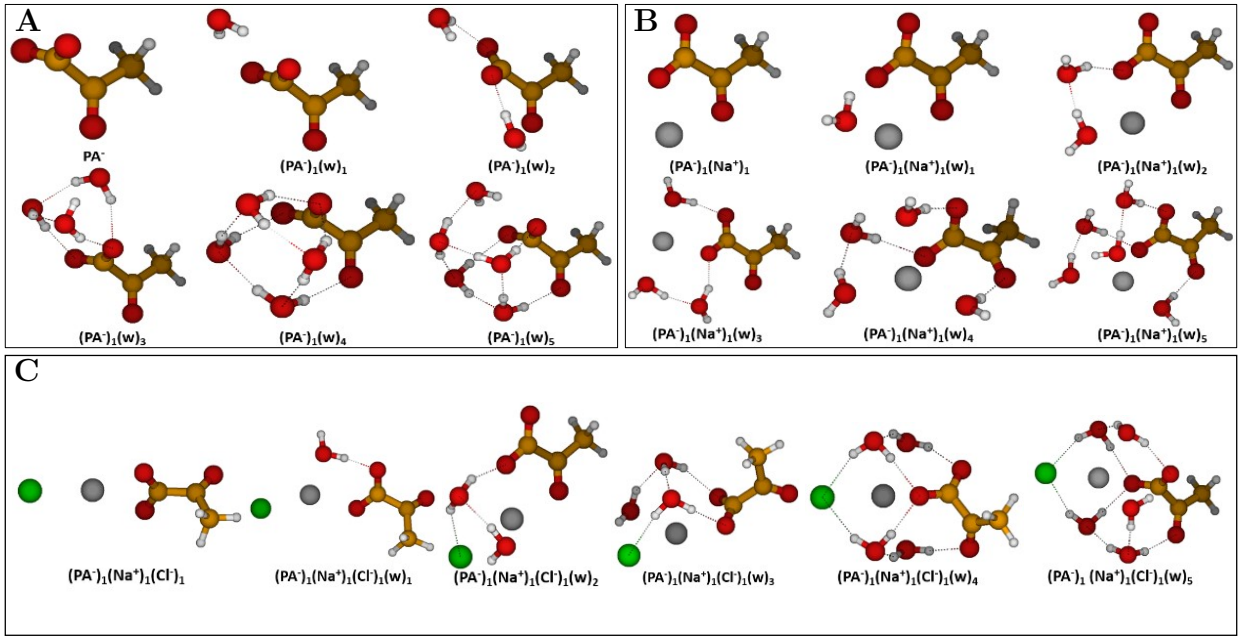

Figure 5: The lowest free energy conformers of pyruvate (PA^-), Na^+, and Cl^- with up to five water (w) molecules: **A** $(PA^-)_1(w)_{0-5}$; **B** $(PA^-)_1(Na^+)_1(w)_{0-5}$; **C** $(PA^-)_1(Na^+)_1(Cl^-)_1(w)_{0-5}$. Calculated at the DLPNO-CCSD(T_0)/aug-cc-pVTZ//ωB97X-D/6-31++G(d,p) level of theory, at 298.15 K and 1 atm using the quasi-harmonic approximation. Hydrogen atoms are white, carbon brown, oxygen red, sodium gray, and chlorine green.

Generally, across all clusters in Figure 5, we observe no proton transfers from water to the PA^- monomer. For the $(PA^-)_1(w)_{0-5}$ clusters in Figure 5**A**, we observed a nascent water hydrogen bonding network forming at the carboxylate terminus of PA^- analogous to our findings for the $(PA)_1(w)_{0-5}$ clusters above.

Upon comparison of the PA^- clusters with literature, we see that both the $(PA^-)_1(w)_1$ and $(PA^-)_1(w)_2$ clusters are consistent with the clusters obtained by Petersen-Sonn et al.[47] obtained at CAM-B3LYP/aug-cc-pVTZ level of theory and the clusters obtained by Shemesh et al.[109] at MP2/cc-pVDZ level of theory. As for the PA clusters examined previously, we observe discrepancies between our $(PA^-)_1(w)_{3-5}$ cluster geometries and literature geometries due to the dispersed water structure in these and as the water structure in our geometries are well-ordered and mainly located at the carboxylate terminus of PA^-.

Upon adding Na^+ to the system in the $(PA^-)_1(Na^+)_1(w)_{0-5}$ clusters of Figure 5**B**, we see that the Na^+ ion preferably interact with the two carbonyl groups instead of the carboxylate group. For the hydrated clusters, the Na^+ ion is seen to bridge the water molecules and the pyruvate ion. This is a similar interaction pattern as observed in the $(PA)_1(Na^+)_1(Cl^-)_1(w)_{0-5}$ clusters of Figure 4**C**.

For the $(PA^-)_1(Na^+)_1(Cl^-)_1(w)_{0-5}$ clusters in Figure 5**C**, we generally observe Na^+ to reside closer to the PA^- monomer where it engages in linear or bifurcated salt bridges with the carboxylate moiety of PA^-. Cl^- is not observed to engage in hydrogen bonds with water or PA^- in the lower hydrated $(PA^-)_1(Na^+)_1(Cl^-)_1$ and $(PA^-)_1(Na^+)_1(Cl^-)_1(w)_1$ clusters due to Coulomb repulsions. However, as more water is added, it becomes increasingly involved in the nascent water hydrogen bonding networks of the higher hydrated clusters. Na^+ is, in this regard, becoming more encapsulated and solvated by the surrounding water, which we also observed for the $(PA)_1(Na^+)_1(Cl^-)_1(w)_{0-5}$ clusters as described above.

3.2 Cluster Binding Free Energies and hydrate distributions

After analyzing the cluster geometries, we progress to probe the binding free energies and hydrate distributions. All calculations are performed at the DLPNO-CCSD(T_0)/aug-cc-pVTZ//ωB97X-D/6-31++G(d,p) level of theory, at 298.15 K and 1 atm using the quasi-harmonic approximation.

3.2.1 The Hydration of Organic Acids

The left panel of Figure 6 presents the gas-phase binding free energy profiles of PA and its various analogs: LA, ProA, and diol. The binding free energies are plotted as a function of "added water molecules", such that each point has the same total number of molecules in the cluster. Hence, zero is the monomer of either the organic acids or a water molecule.

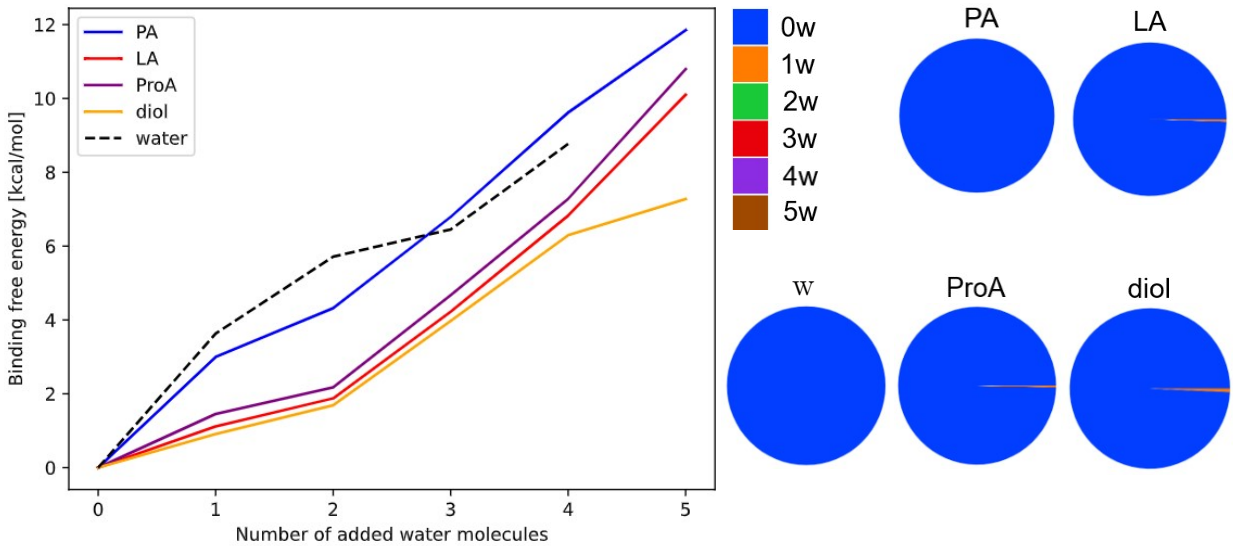

Figure 6: Left: Binding free energies of $(PA)_1(w)_{0-5}$ (blue), $(LA)_1(w)_{0-5}$ (red), $(ProA)_1(w)_{0-5}$ (purple), and $(diol)_1(w)_{0-5}$ (orange) at 298.15 K with the binding free energies of pure water clusters at the given level of theory included as a black dashed line. Right: Equilibrium hydrate distributions of the various organic acids and the water reference at 298.15 K and 1 atm and at 100% relative humidity.

All binding free energies are positive and increase with the number of water molecules in the cluster. This entails that the clusters become increasingly more thermodynamically unfavorable and thus increasingly unstable in the gas-phase when adding more water molecules. This is most pronounced for the $(PA)_1(w)_{0-5}$ clusters as they are observed to be close to or even higher in free energy compared to the pure gas-phase water clusters. The higher free energy is caused by the internal H-bond present in the PA monomer. Hence, to form clusters with water, PA needs to break the internal H-bond, which thereby does not lead to a gain in free energy.

The first hydration steps of LA, ProA, and diol is more favorable compared to PA. In addition, the binding free energies are very similar for the addition of the first four water molecules. However, the addition of the fifth water molecule is significantly more favorable for the diol compared to LA and ProA. This can be rationalized from the structures in Figure 3, where the diol is interacting with all five water molecules in the extended H-bond network, while LA and ProA primarily interact with four water molecules and have the fifth water molecule only interacting with other water molecules and not the acids.

The right panel of Figure 6 presents the hydrate distributions of the organic acids. All the organic acids are observed to be non-hydrated in the gas-phase. Hydrate distributions obtained at 273.15 K and 258.15 K and at 50% relative humidity does not change this conclusion (see Supporting Information).

The fact that the clusters do not interact favorably with up to five water molecules could indicate that more water molecules are needed to describe how small chain organic acids enter an aerosol particle. Alternatively, this could also indicate that an aqueous surface should potentially include ions to thermodynamically stabilize the clusters.

3.2.2 The Pyruvic Acid-Containing Clusters

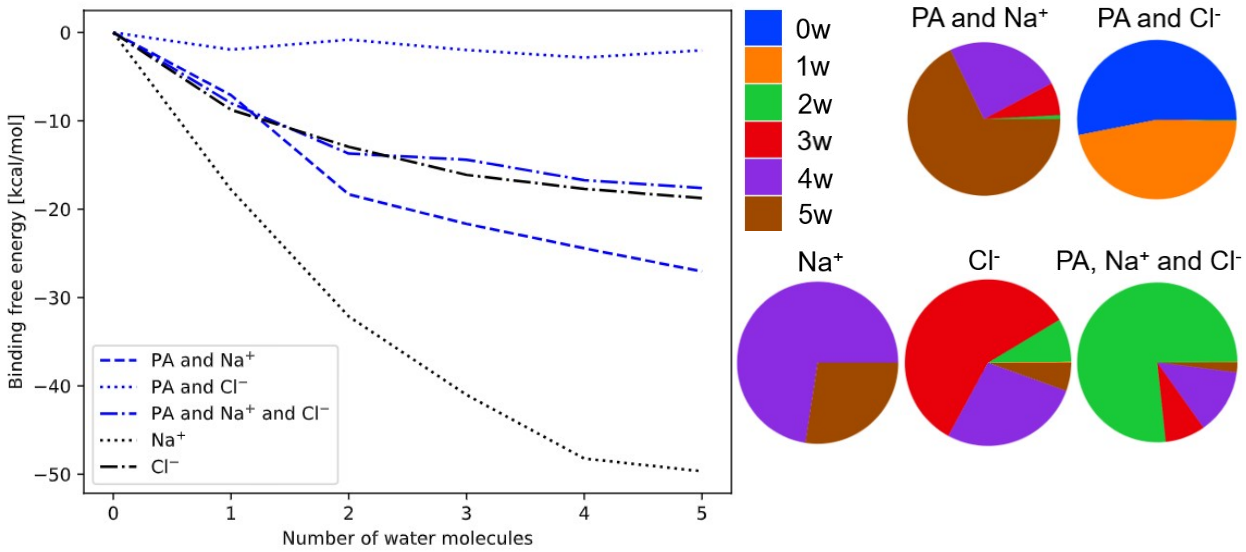

Figure 7: Left: Normalized binding free energies with respect to the dry clusters of $(PA)_1(Na^+)_1(w)_{0-5}$ (blue dashed), $(PA)_1(Cl^-)_1(w)_{0-5}$ (blue dotted), and $(PA)_1(Na^+)_1(Cl^-)_1(w)_{0-5}$ (blue dash-dotted) at 298.15 K and with the binding free energies of the reference $(Na^+)_1(w)_{0-5}$ and $(Cl^-)_1(w)_{0-5}$ clusters at the given level of theory included as a black dotted and a black dashdotted line, respectively. Right: Equilibrium hydrate distributions of the various clusters at 298.15 K and 1 atm and at 100% relative humidity.

The binding free energy profiles of the PA clusters containing Na^+ and Cl^- ions were investigated. The left panel of Figure 7 presents the gas-phase binding free energies of PA with Na^+ and Cl^-. In contrast to the positive binding free energies of the hydrated clusters containing PA, LA, ProA, and diol as discussed above, we generally observe the hydrated PA clusters containing ions to be thermodynamically favorable. Especially the $(PA)_1(Na^+)_1(w)_{0-5}$ and the $(PA)_1(Na^+)_1(Cl^-)_1(w)_{0-5}$ clusters are seen to decrease markedly at smaller water content and then flatten out at larger water content. This indicates that the stabilizing effect is diminishing with increasing water content. On the other hand, the $(PA)_1(Cl^-)_1(w)_{0-5}$ clusters are observed to be relatively constant, just below zero in normalized binding free energy,

which indicates that Cl^- is not able to thermodynamically stabilize the hydrated clusters in the gas-phase as favorably as the hydrated clusters containing Na^+. Generally, the hydration of the pyruvic acid-containing clusters in the presence of ions is negative and thus the ions may compensate for the lack of binding observed in the pure PA–water clusters. In the case of $(PA)_1(Cl^-)_1(w)_{0-5}$, the binding free energy is nearly zero as the negative free energy of the $(Cl^-)_1(w)_{0-5}$ clusters cancel with the positive free energy of the $(PA)_1(w)_{0-5}$ clusters. In the case of the $(PA)_1(Na^+)_1(w)_{0-5}$ clusters, the presence of the Na^+ ion still leads to a low free energy.

The right panel of Figure 7 presents the hydrate distributions of the pyruvic acid-containing clusters. Generally, we observe the highly hydrated clusters to be favored when the binding free energy is very negative and we observe the $(PA)_1(Na^+)_1(w)_{0-5}$ clusters to favor hydration the most. Similar conclusion is reached when studying the hydrate distributions obtained at 273.15 K and 258.15 K and at 50% relative humidity (available in the Supporting Information).

Generally, when comparing the binding free energy analysis and the hydrate distributions with the cluster geometry analysis in the previous section, it is clear that Na^+ ions stabilize the PA clusters the most and the stabilization is less pronounced for the Cl^- ion. Furthermore, a significant degree of solvation of the Na^+ ion by water in the gas-phase is also thermodynamically favorable for stabilizing the clusters.

3.2.3 The Pyruvate-Containing Clusters

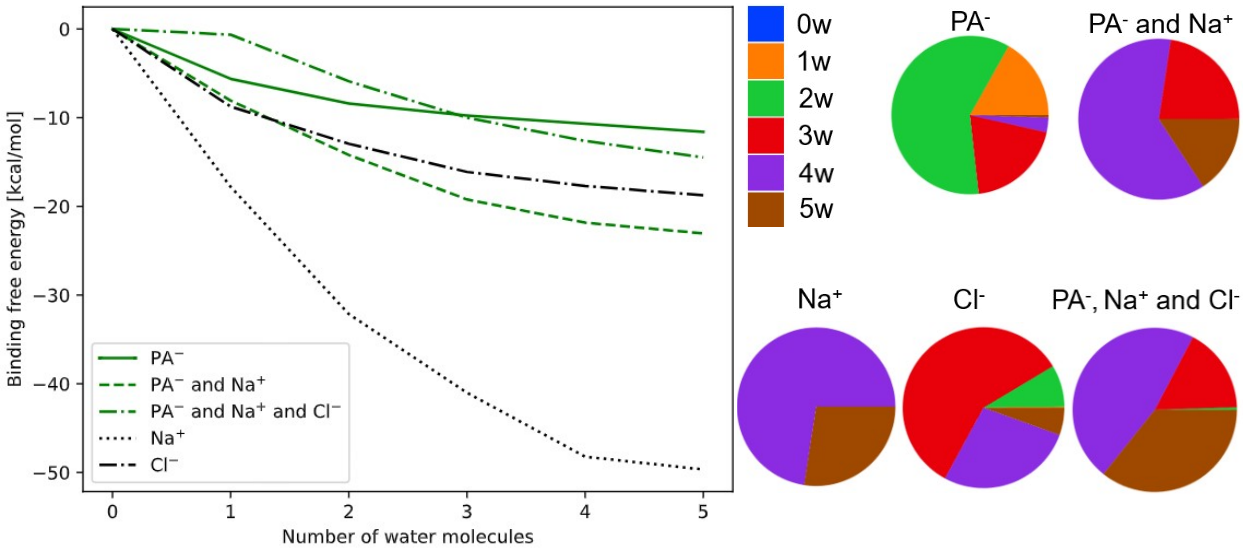

Figure 8: Left: Normalized binding free energies with respect to the dry clusters of $(PA^-)_1(w)_{0-5}$, $(PA^-)_1(Na^+)_1(w)_{0-5}$, and $(PA^-)_1(Na^+)_1(Cl^-)_1(w)_{0-5}$ at 298.15 K. Right: Equilibrium hydrate distributions of the various clusters at 298.15 K and 1 atm and at 100% relative humidity.

Deprotonation of PA leading to PA^- could lead to more stable clusters. The left panel of Figure 8 presents the binding free energies normalized to the dry clusters of PA^- with Na^+ and Cl^-. Generally, the hydration profiles are similar to the PA-containing clusters described above. We observe the energies of the $(PA^-)_1(w)_{0-5}$, $(PA^-)_1(Na^+)_1(w)_{0-5}$ and $(PA^-)_1(Na^+)_1(Cl^-)_1(w)_{0-5}$ to decrease with increasing water content. This leads to negative binding free energies in all cases. Hence, pyruvate hydration is favorable and, in general, seems to be enhanced by other ions.

The right panel of Figure 8 presents the hydrate distributions of the pyruvate-containing clusters. In all cases, the clusters are highly hydrated with 2–5 water molecules. The $(PA^-)_1(Na^+)_1(Cl^-)_1(w)_{0-5}$ clusters are found to be slightly more hydrated than the corresponding $(PA^-)_1(Na^+)_1(w)_{0-5}$ clusters. This could indicate that Cl^- exhibits a synergistic

effect with Na^+ in thermodynamically stabilizing the higher hydrated clusters. Hydrate distributions obtained at 273.15 K and 258.15 K and at 50% relative humidity show similar trends (see Supporting Information).

Overall, we find that ions are very important for the interaction between the PA monomer and water as well as between the PA^- monomer and water addressed here. Hence, for organics to efficiently partition to the particle-phase some surface ions should most likely be present.

3.3 IR Absorption

Gas-phase measurements of hydrated clusters are extremely difficult to carry out. One promising technique to identify weakly bound clusters is to probe the H-shift of the O–H stretch upon cluster formation. This methodology has been applied to detect clusters such as the gas-phase PA monomer,[63] the gas-phase dimethylamine monomer,[110] and the gas-phase methanol–dimethylamine dimer[111] where the N–H stretch is contributing to cluster formation. However, to the best of our knowledge, there are no previous studies on the IR absorptions of hydrated PA clusters in the gas-phase. Here we provide such analysis to potentially guide future experiments. The IR spectra presented in this section were obtained at ωB97X-D/6-31++G(d,p) level of theory. We stress that the choice of method is qualitatively sufficient for the following analysis. I.e. the peaks in the IR spectra are likely shifted compared experimental values, but the overall relative peak positions should accurate.

3.3.1 IR Absorption of the Hydrated Pyruvic Acid Clusters

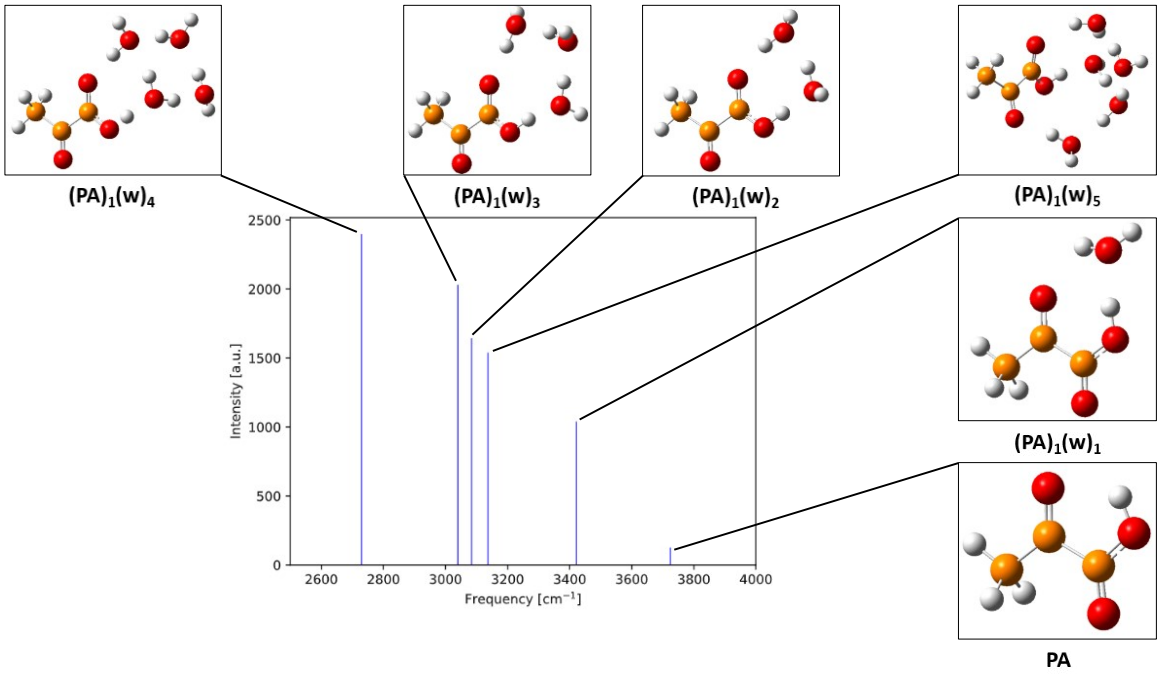

Figure 9: IR intensities as a function of IR O–H frequencies corresponding to the carboxylic O–H stretching vibration of PA for $(PA)_1(w)_{0-5}$. Hydrogen atoms are white, carbon brown, and oxygen red.

Figure 9 presents the IR O–H frequencies and intensities of the hydrated gas-phase PA clusters with the corresponding cluster geometries. Generally, we see a trend of decreasing O–H frequency (red-shift) and increasing intensity with increasing cluster water content. As the PA monomer is found not to be hydrated in the gas-phase a strong red-shift from 3725 cm^{-1} in an experiment could indicate that the PA monomer is interacting with one or more water molecules. This streching frequency mode for the gas-phase PA monomer is also in fairly good agreement with previously reported experimental work.[63]

3.3.2 IR Absorption of the Clusters Containing Pyruvic Acid and Na^+

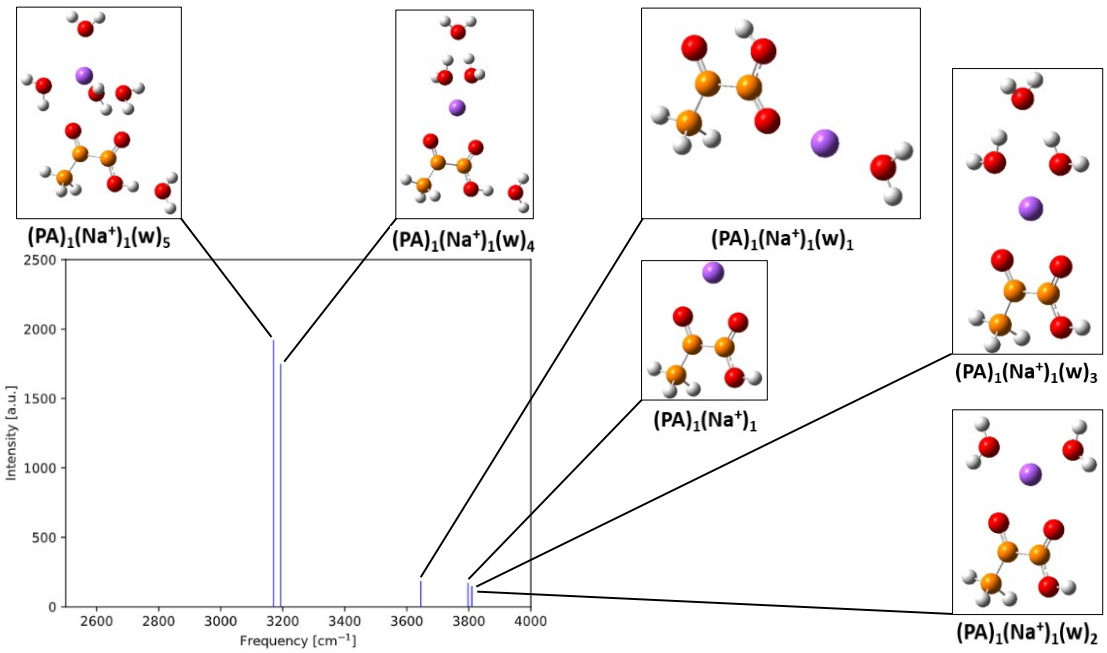

Figure 10: IR intensities as a function of IR O–H frequencies for $(PA)_1(Na^+)_1(w)_{0-5}$. Hydrogen atoms are white, carbon brown, oxygen red, and sodium purple.

Figure 10 presents the IR O–H frequencies and intensities of the hydrated gas-phase PA clusters with Na^+. In contrast to the hydrated PA clusters described above, we generally observe a more mixed pattern in O–H frequencies with respect to cluster water content. The difference in intensities in the spectrum can be attributed to the presence of water at the O–H bond, as seen in the $(PA)_1(Na^+)_1(w)_4$ and $(PA)_1(Na^+)_1(w)_5$ clusters, with red-shifts of 532 cm^{-1} and 555 cm^{-1} compared to the PA monomer, respectively. The remaining clusters do not have water present at the O–H bond, which leads to an O–H stretching frequency similar to the isolated PA monomer.

3.3.3 IR Absorptions of the Clusters Containing Pyruvic Acid and Cl^-

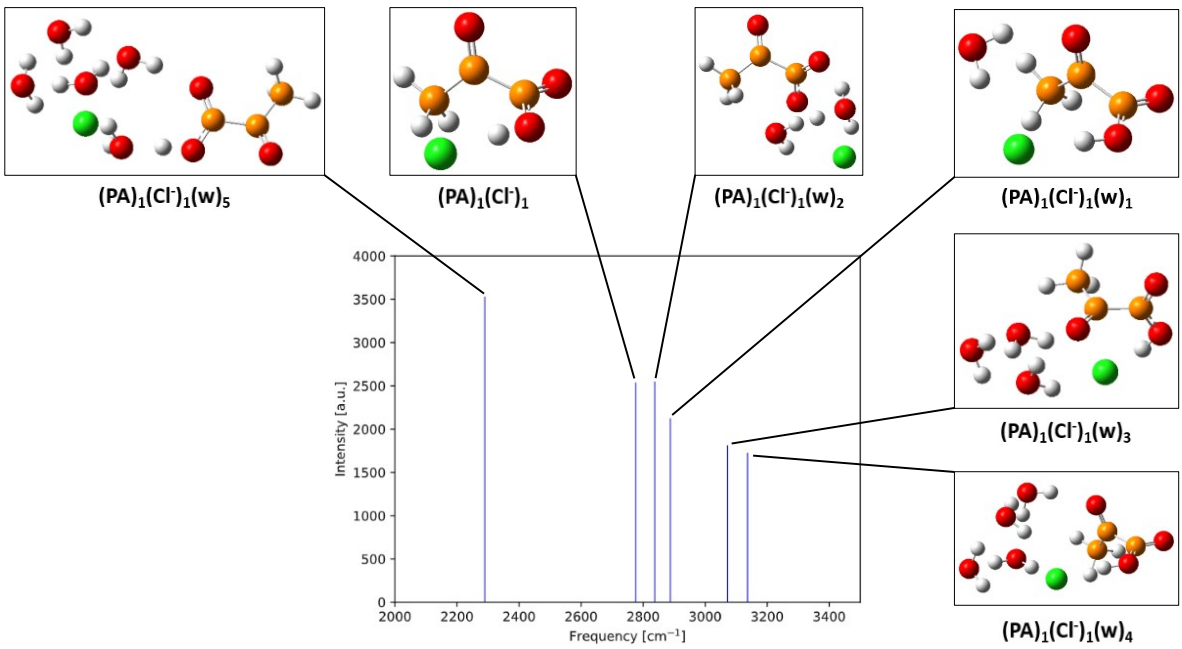

Figure 11: IR intensities as a function of IR O–H frequencies for $(PA)_1(Cl\text{-})_1(w)_{0-5}$. Hydrogen atoms are white, carbon brown, oxygen red, and chlorine green.

Figure 11 shows the IR O–H frequencies and intensities of the hydrated gas-phase PA clusters with Cl^-. We generally observe the O–H frequency pattern with respect to water content to be even more mixed here than for the $(PA)_1(Na^+)_1(w)_{0-5}$ clusters. The O–H stretching frequency is significantly red-shifted (by up to 1435 cm^{-1}) compared to the PA monomer in all cases. This is caused by the strong interaction between the Cl^- ion and the O–H group. Hence, a very strong red-shift in the IR-spectrum could indicate the presence of a tight ion-pair with chloride ion.

3.3.4 IR Absorption of the Clusters Containing Pyruvic Acid, Na^+, and Cl^-

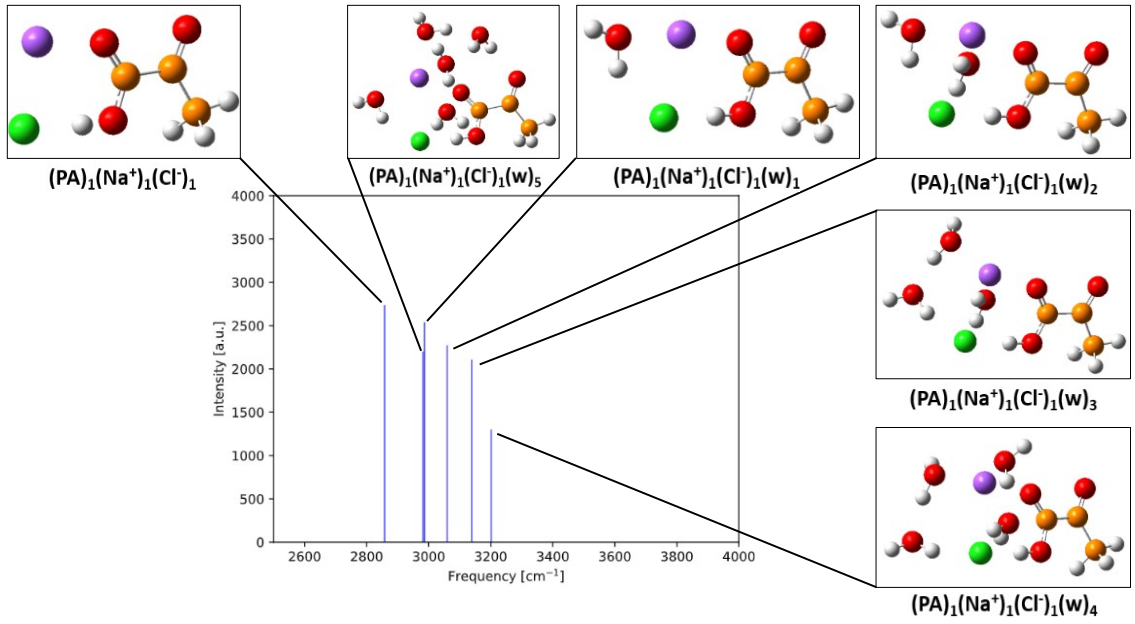

Figure 12: IR intensities as a function of IR O–H frequencies for $(PA)_1(Na^+)_1(Cl\text{-})_1(w)_{0-5}$. Hydrogen atoms are white, carbon brown, oxygen red, sodium purple, and chlorine green.

Figure 12 shows the IR intensities as a function of IR O–H frequencies of the hydrated gas-phase clusters with Na^+ and Cl^-. All the clusters are red-shifted by up to 867 cm^{-1} compared to the PA monomer. In addition, we observe the O–H frequencies to increase with increasing water content while the intensities decrease. This is in contrast to the hydrated PA clusters with no ions present.

To summarize the above IR analyses of the various systems, we can corroborate the correlation between decreasing O–H frequency and increasing intensity with increasing water content of the clusters, which is gradually reversed when adding ions to the system. Finally, we see a propensity toward red-shifting of the O–H vibrational frequencies when adding more ions to the hydrated PA clusters even though the O–H frequencies in the $(PA)_1(Na^+)_1(w)_{0-5}$ clusters resonate consistently above 3000 cm^{-1}.

4 Conclusions

Here we have studied the molecular interaction between organic acids, water and ions at a mimic aerosol surface. In our study of the cluster geometries of the reference systems comprised of pure water, hydrated Na^+, and hydrated Cl^-, we find that all are in full agreement with literature. This illustrates the applicability of the applied computational approach.

For the cluster geometries of hydrated pyruvate and organic acids (including pyruvic acid), we show that for all clusters containing one to four water molecules, a complete conservation of the water network structure with respect to the pure water cluster is preserved. However, upon introduction of ions into the pyruvic acid-containing clusters and pyruvate-containing clusters, we show that the water structure of the clusters are perturbed significantly compared to the organic acid clusters without ions and the reference systems.

In our investigation of the cluster binding free energies and hydrate distributions, we find that the organic acids PA, LA, ProA, and diol are not hydrated in the gas-phase. On the other hand, we find that the pyruvic-acid containing clusters and the pyruvate-containing clusters with ions present are significantly more thermodynamically stabilized in the gas-phase with the Na^+ ion contributing the most to this stabilization. This suggests that for organic acids, to efficiently transition from the gas-phase to the particle-phase, some interfacial surface ions should possibly be present to facilitate the process.

As a part of the IR absorption studies of the various pyruvic-acid containing clusters, we find a correlation between decreasing O–H frequency and increasing intensity when more water is added to the clusters. Furthermore, we observe a correlation between increasing red-shift of the O–H frequencies upon addition of ions to the clusters indicating strong interactions between the PA monomer and the surrounding water and ions.

In the following work to this study, we will investigate the same systems in the aqueous phase and at aerosol surfaces to probe the cluster geometries and stabilities when changing the chemical environment. Thereby we can fully unravel the mechanisms, which leads to

favorable partitioning of organic acids into aerosol particles, where they can contribute to atmospheric particle growth.

Acknowledgement

This work was funded by the Danish National Research Foundation (DNRF172) through the Center of Excellence for Chemistry of Clouds and by the European Union (MSCA, HYDRO-CLUSTER, project 101105506). Views and opinions expressed are however those of the authors only and do not necessarily reflect those of the European Union or the European Research Council Executive Agency. Neither the European Union nor the granting authority can be held responsible for them.

The numerical results presented in this work were obtained at the Centre for Scientific Computing, Aarhushttps://phys.au.dk/forskning/faciliteter/cscaa/. We would like to thank PhD student Yosef Knattrup for his contributions to the generation of JKCS input files for the various conformers of lactic acid. Also, we would like to thank Postdoc Eva R. Kjærgaard for her contributions to creating the TOC figure.

Supporting Information Available

The following is available as supporting information:

The assessment of pyruvic acid conformers; The assessment of pyruvic acid interaction energies; Initial benchmark results; Cluster binding free energies and hydrate distributions at various temperatures.

References

(1) Lund Myhre, C. E.; Nielsen, C. J. Optical Properties in the UV and Visible Spectral Region of Organic Acids Relevant to Tropospheric Aerosols. *Atmos. Chem. Phys.* **2004**, *4*, 1759–1769.

(2) Eger, P. G.; Schuladen, J.; Sobanski, N.; Fischer, H.; Karu, E.; Williams, J.; Riva, M.; Zha, Q.; Ehn, M.; Quéléver, L. L. J.; Schallhart, S.; Lelieveld, J.; Crowley, J. N. Pyruvic Acid in the Boreal Forest: Gas-Phase Mixing Ratios and Impact on Radical Chemistry. *Atmos. Chem. Phys.* **2020**, *20*, 3697–3711.

(3) Kawamura, K.; Tachibana, E.; Okuzawa, K.; Aggarwal, S. G.; Kanaya, Y.; Wang, Z. F. High Abundances of Water-Soluble Dicarboxylic Acids, Ketocarboxylic Acids and α-Dicarbonyls in the Mountaintop Aerosols over the North China Plain during Wheat Burning Season. *Atmos. Chem. Phys.* **2013**, *13*, 8285–8302.

(4) Kawamura, K.; Bikkina, S. A Review of Dicarboxylic Acids and Related Compounds in Atmospheric Aerosols: Molecular Distributions, Sources and Transformation. *Atmos. Res.* **2016**, *170*, 140–160.

(5) Kawamura, K.; Yasui, O. Diurnal Changes in the Distribution of Dicarboxylic Acids, Ketocarboxylic Acids and Dicarbonyls in the Urban Tokyo Atmosphere. *Atmos. Environ.* **2005**, *39*, 1945–1960.

(6) Ho, K. F.; Lee, S. C.; Cao, J. J.; Kawamura, K.; Watanabe, T.; Cheng, Y.; Chow, J. C. Dicarboxylic Acids, Ketocarboxylic Acids and Dicarbonyls in the Urban Roadside Area of Hong Kong. *Atmos. Environ.* **2006**, *40*, 3030–3040.

(7) Ho, K. F.; Cao, J. J.; Lee, S. C.; Kawamura, K.; Zhang, R. J.; Chow, J. C.; Watson, J. G. Dicarboxylic Acids, Ketocarboxylic Acids, and Dicarbonyls in the Urban Atmosphere of China. *J. Geophys. Res. Atmos.* **2007**, *112*.

(8) Ho, K. F.; Lee, S. C.; Ho, S. S. H.; Kawamura, K.; Tachibana, E.; Cheng, Y.; Zhu, T. Dicarboxylic Acids, Ketocarboxylic Acids, α-Dicarbonyls, Fatty Acids, and Benzoic Acid in Urban Aerosols Collected during the 2006 Campaign of Air Quality Research in Beijing (CAREBeijing-2006). *J. Geophys. Res. Atmos.* **2010**, *115*.

(9) Jung, J.; Tsatsral, B.; Kim, Y. J.; Kawamura, K. Organic and Inorganic Aerosol Compositions in Ulaanbaatar, Mongolia, during the Cold Winter of 2007 to 2008: Dicarboxylic Acids, Ketocarboxylic Acids, and α-Dicarbonyls. *J. Geophys. Res. Atmos.* **2010**, *115*.

(10) Pavuluri, C. M.; Kawamura, K.; Swaminathan, T. Water-Soluble Organic Carbon, Dicarboxylic Acids, Ketoacids, and α-Dicarbonyls in the Tropical Indian Aerosols. *J. Geophys. Res. Atmos.* **2010**, *115*.

(11) Kawamura, K. Identification of C2–C10 ω-oxocarboxylic acids, pyruvic acid, and C2–C3 α-Dicarbonyls in Wet Precipitation and Aerosol Samples by Capillary GC and GC/MS. *Anal. Chem.* **1993**, *65*, 3505–3511.

(12) Wang, H.; Kawamura, K.; Yamazaki, K. Water-Soluble Dicarboxylic Acids, Ketoacids and Dicarbonyls in the Atmospheric Aerosols over the Southern Ocean and Western Pacific Ocean. *J. Atmos. Chem.* **2006**, *53*, 43–61.

(13) Fu, P.; Kawamura, K.; Usukura, K.; Miura, K. Dicarboxylic Acids, Ketocarboxylic Acids and Glyoxal in the Marine Aerosols Collected during a Round-The-World Cruise. *Mar. Chem.* **2013**, *148*, 22–32.

(14) Kawamura, K.; Kasukabe, H.; Barrie, L. A. Secondary Formation of Water-Soluble Organic Acids and α-Dicarbonyls and Their Contributions to Total Carbon and Water-Soluble Organic Carbon: Photochemical Aging of Organic Aerosols in the Arctic Spring. *J. Geophys. Res. Atmos.* **2010**, *115*.

(15) Kundu, S.; Kawamura, K.; Andreae, T. W.; Hoffer, A.; Andreae, M. O. Molecular Distributions of Dicarboxylic Acids, Ketocarboxylic Acids and α-Dicarbonyls in Biomass Burning Aerosols: Implications for Photochemical Production and Degradation in Smoke Layers. *Atmos. Chem. Phys.* **2010**, *10*, 2209–2225.

(16) Griffith, E. C.; Carpenter, B. K.; Shoemaker, R. K.; Vaida, V. Photochemistry of Aqueous Pyruvic Acid. *Proc. Natl. Acad. Sci.* **2013**, *110*, 11714–11719.

(17) Reed Harris, A. E.; Ervens, B.; Shoemaker, R. K.; Kroll, J. A.; Rapf, R. J.; Griffith, E. C.; Monod, A.; Vaida, V. Photochemical Kinetics of Pyruvic Acid in Aqueous Solution. *J. Phys. Chem. A* **2014**, *118*, 8505–8516.

(18) Eugene, A. J.; Guzman, M. I. Reactivity of Ketyl and Acetyl Radicals from Direct Solar Actinic Photolysis of Aqueous Pyruvic Acid. *J. Phys. Chem. A* **2017**, *121*, 2924–2935.

(19) Rapf, R. J.; Perkins, R. J.; Carpenter, B. K.; Vaida, V. Mechanistic Description of Photochemical Oligomer Formation from Aqueous Pyruvic Acid. *J. Phys. Chem. A* **2017**, *121*, 4272–4282.

(20) Rapf, R. J.; Dooley, M. R.; Kappes, K.; Perkins, R. J.; Vaida, V. pH Dependence of the Aqueous Photochemistry of α-Keto Acids. *J. Phys. Chem. A* **2017**, *121*, 8368–8379.

(21) Maroń, M. K.; Takahashi, K.; Shoemaker, R. K.; Vaida, V. Hydration of Pyruvic Acid to its Geminal-Diol, 2, 2-Dihydroxypropanoic Acid, in a Water-Restricted Environment. *Chem. Phys. Lett.* **2011**, *513*, 184–190.

(22) Guzman, M. I.; Colussi, A. J.; Hoffmann, M. R. Photoinduced Oligomerization of Aqueous Pyruvic Acid. *J. Phys. Chem. A* **2006**, *110*, 3619–3626.

(23) Ault, A. P. Aerosol Acidity: Novel Measurements and Implications for Atmospheric Chemistry. *Acc. Chem. Res.* **2020**, *53*, 1703–1714.

(24) Reed Harris, A. E.; Pajunoja, A.; Cazaunau, M.; Gratien, A.; Pangui, E.; Monod, A.; Griffith, E. C.; Virtanen, A.; Doussin, J.-F.; Vaida, V. Multiphase Photochemistry of Pyruvic Acid under Atmospheric Conditions. *J. Phys. Chem. A* **2017**, *121*, 3327–3339.

(25) Kappes, K. J.; Deal, A. M.; Jespersen, M. F.; Blair, S. L.; Doussin, J.-F.; Cazaunau, M.; Pangui, E.; Hopper, B. N.; Johnson, M. S.; Vaida, V. Chemistry and Photochemistry of Pyruvic Acid at the Air–Water Interface. *J. Phys. Chem. A* **2021**, *125*, 1036–1049.

(26) Yamamoto, S.; Back, R. A. The Photolysis and Thermal Decomposition of Pyruvic Acid in the Gas Phase. *Can. J. Chem.* **1985**, *63*, 549–554.

(27) Andreae, M. O.; Talbot, R. W.; Li, S.-M. Atmospheric Measurements of Pyruvic and Formic Acid. *J. Geophys. Res. Atmos.* **1987**, *92*, 6635–6641.

(28) Takahashi, K.; Plath, K. L.; Skodje, R. T.; Vaida, V. Dynamics of Vibrational Overtone Excited Pyruvic Acid in the Gas Phase: Line Broadening through Hydrogen-Atom Chattering. *J. Phys. Chem. A* **2008**, *112*, 7321–7331.

(29) Plath, K. L.; Takahashi, K.; Skodje, R. T.; Vaida, V. Fundamental and Overtone Vibrational Spectra of Gas-Phase Pyruvic Acid. *J. Phys. Chem. A* **2009**, *113*, 7294–7303.

(30) Reed Harris, A. E.; Doussin, J.-F.; Carpenter, B. K.; Vaida, V. Gas-Phase Photolysis of Pyruvic Acid: The Effect of Pressure on Reaction Rates and Products. *J. Phys. Chem. A* **2016**, *120*, 10123–10133.

(31) Jacob, D. J.; Wofsy, S. C. Photochemistry of Biogenic Emissions over the Amazon Forest. *J. Geophys. Res. Atmos.* **1988**, *93*, 1477–1486.

(32) Grosjean, D.; Williams, E. L.; Grosjean, E. Atmospheric Chemistry of Isoprene and of its Carbonyl Products. *Environ. Sci. Technol.* **1993**, *27*, 830–840.

(33) Paulot, F.; Crounse, J. D.; Kjaergaard, H. G.; Kroll, J. H.; Seinfeld, J. H.; Wennberg, P. O. Isoprene Photooxidation: New Insights into the Production of Acids and Organic Nitrates. *Atmos. Chem. Phys.* **2009**, *9*, 1479–1501.

(34) Raber, W. H.; Moortgat, G. K. Photooxidation of Selected Carbonyl Compounds in Air: Methyl Ethyl Ketone, Methyl Vinyl Ketone, Methacrolein and Methylglyoxal. *Progress and problems in atmospheric chemistry, edited by: Barker, J. R., World Scientific Publishing, Singapore* **1995**, 318–373.

(35) Jenkin, M. E.; Cox, R. A.; Emrich, M.; Moortgat, G. K. Mechanisms of the Cl-Atom-Initiated Oxidation of Acetone and Hydroxyacetone in Air. *J. Chem. Soc. Faraday Trans.* **1993**, *89*, 2983–2991.

(36) Warneck, P. Multi-Phase Chemistry of C_2 and C_3 Organic Compounds in the Marine Atmosphere. *J. Atmos. Chem.* **2005**, *51*, 119–159.

(37) Grosjean, D. Atmospheric Reactions of Ortho Cresol: Gas Phase and Aerosol Products. *Atmos. Environ.* **1984**, *18*, 1641–1652.

(38) Praplan, A. P.; Hegyi-Gaeggeler, K.; Barmet, P.; Pfaffenberger, L.; Dommen, J.; Baltensperger, U. Online Measurements of Water-Soluble Organic Acids in the Gas and Aerosol Phase from the Photooxidation of 1,3,5-Trimethylbenzene. *Atmos. Chem. Phys.* **2014**, *14*, 8665–8677.

(39) Horowitz, A.; Meller, R.; Moortgat, G. K. The UV–VIS Absorption Cross Sections of the α-Dicarbonyl Compounds: Pyruvic Acid, Biacetyl and Glyoxal. *J. Photochem. Photobiol. A* **2001**, *146*, 19–27.

(40) Carlton, A. G.; Turpin, B. J.; Lim, H.-J.; Altieri, K. E.; Seitzinger, S. Link between Isoprene and Secondary Organic Aerosol (SOA): Pyruvic Acid Oxidation Yields Low Volatility Organic Acids in Clouds. *Geophys. Res. Lett.* **2006**, *33*.

(41) Tan, Y.; Lim, Y. B.; Altieri, K. E.; Seitzinger, S. P.; Turpin, B. J. Mechanisms Leading to Oligomers and SOA through Aqueous Photooxidation: Insights from OH Radical Oxidation of Acetic Acid and Methylglyoxal. *Atmos. Chem. Phys.* **2012**, *12*, 801–813.

(42) Eugene, A. J.; Guzman, M. I. The Effects of Reactant Concentration and Air Flow Rate in the Consumption of Dissolved O_2 during the Photochemistry of Aqueous Pyruvic Acid. *Molecules* **2019**, *24*, 1124.

(43) Mekic, M.; Liu, J.; Zhou, W.; Loisel, G.; Cai, J.; He, T.; Jiang, B.; Yu, Z.; Lazarou, Y. G.; Li, X.; Brigante, M.; Vione, D.; Gligorovski, S. Formation of Highly Oxygenated Multifunctional Compounds from Cross-Reactions of Carbonyl Compounds in the Atmospheric Aqueous Phase. *Atmos. Environ.* **2019**, *219*, 117046.

(44) Grosjean, D. Atmospheric Reactions of Pyruvic Acid. *Atmos. Environ.* **1983**, *17*, 2379–2382.

(45) Winterhalter, R.; Jensen, N. R.; Magneron, I.; Wirtz, K.; Mellouki, W.; Yuying, M.; Tadic, J.; Horowitz, A.; Moortgat, G. K.; Hjorth, J. Studies of the Photolysis of Pyruvic Acid: Products and Mechanism. *Proceedings of the EUROTRAC-2 Symposium 2000 on "Transport and Chemical Transformation in the Troposphere, edited by: Midgley, P. M., Reuther, M., and Williams, M., Garmisch Partenkirchen, 2000, Springer, Berlin* **2001**,

(46) Mellouki, A.; Mu, Y. On the Atmospheric Degradation of Pyruvic Acid in the Gas Phase. *J. Photochem. Photobiol. A* **2003**, *157*, 295–300.

(47) Petersen-Sonn, E. A.; Jespersen, M. F.; Johnson, M. S.; Mikkelsen, K. V. Mechanistic Insights into UV Spectral Changes of Pyruvic Acid and Pyruvate Part 1: Interaction with Water Molecules. *Int. J. Phys. Res.* **2024**, *7*, 100–107.

(48) Zhang, J.; Dolg, M. ABCluster: The Artificial Bee Colony Algorithm for Cluster Global Optimization. *Phys. Chem. Chem. Phys.* **2015**, *17*, 24173–24181.

(49) Zhang, J.; Dolg, M. Global Optimization of Clusters of Rigid Molecules Using the Artificial Bee Colony Algorithm. *Phys. Chem. Chem. Phys.* **2016**, *18*, 3003–3010.

(50) Grimme, S.; Bannwarth, C.; Shushkov, P. A Robust and Accurate Tight-Binding Quantum Chemical Method for Structures, Vibrational Frequencies, and Noncovalent Interactions of Large Molecular Systems Parametrized for All spd-Block Elements (Z= 1–86). *J. Chem. Theory Comput.* **2017**, *13*, 1989–2009.

(51) Bannwarth, C.; Caldeweyher, E.; Ehlert, S.; Hansen, A.; Pracht, P.; Seibert, J.; Spicher, S.; Grimme, S. Extended Tight-Binding Quantum Chemistry Methods. *Wiley Interdiscip. Rev. Comput. Mol. Sci.* **2021**, *11*, e1493.

(52) Frisch, M. et al. Gaussian 16 Revision B.01. 2016; Gaussian Inc. Wallingford CT.

(53) Neese, F. Software Update: The ORCA Program System—Version 5.0. *Wiley Interdiscip. Rev. Comput. Mol. Sci.* **2022**, *12*, e1606.

(54) Kubecka, J.; Neefjes, I.; Besel, V.; Qiao, F.; Xie, H.-B.; Elm, J. Atmospheric Sulfuric Acid–Multi-Base New Particle Formation Revealed through Quantum Chemistry Enhanced by Machine Learning. *J. Phys. Chem. A* **2023**, *127*, 2091–2103.

(55) Elm, J. Clusteromics I: Principles, Protocols, and Applications to Sulfuric Acid–Base Cluster Formation. *ACS Omega* **2021**, *6*, 7804–7814.

(56) Elm, J. Clusteromics II: Methanesulfonic Acid–Base Cluster Formation. *ACS Omega* **2021**, *6*, 17035–17044.

(57) Elm, J. Clusteromics III: Acid Synergy in Sulfuric Acid–Methanesulfonic Acid–Base Cluster Formation. *ACS Omega* **2022**, *7*, 15206–15214.

(58) Knattrup, Y.; Elm, J. Clusteromics IV: The Role of Nitric Acid in Atmospheric Cluster Formation. *ACS Omega* **2022**, *7*, 31551–31560.

(59) Jensen, A. B.; Kubecka, J.; Schmitz, G.; Christiansen, O.; Elm, J. Massive Assessment of the Binding Energies of Atmospheric Molecular Clusters. *J. Chem. Theory Comput.* **2022**, *18*, 7373–7383.

(60) Ayoubi, D.; Knattrup, Y.; Elm, J. Clusteromics V: Organic Enhanced Atmospheric Cluster Formation. *ACS Omega* **2023**, *8*, 9621–9629.

(61) Engsvang, M.; Wu, H.; Elm, J. Iodine Clusters in the Atmosphere I: Computational Benchmark and Dimer Formation of Oxyacids and Oxides. *ACS Omega* **2024**, *9*, 31521–31532.

(62) Kubecka, J.; Besel, V.; Neefjes, I.; Knattrup, Y.; Kurtén, T.; Vehkamäki, H.; Elm, J. Computational Tools for Handling Molecular Clusters: Configurational Sampling, Storage, Analysis, and Machine Learning. *ACS Omega* **2023**, *8*, 45115–45128.

(63) Blair, S. L.; Reed Harris, A. E.; Frandsen, B. N.; Kjaergaard, H. G.; Pangui, E.; Cazaunau, M.; Doussin, J.-F.; Vaida, V. Conformer-Specific Photolysis of Pyruvic Acid and the Effect of Water. *J. Phys. Chem. A* **2020**, *124*, 1240–1252.

(64) Borba, A.; Gómez-Zavaglia, A.; Lapinski, L.; Fausto, R. Rotational Isomers of Lactic Acid: First Experimental Observation of Higher Energy Forms. *Phys. Chem. Chem. Phys.* **2004**, *6*, 2101–2108.

(65) Zhang, J. Atom Typing Using Graph Representation Learning: How Do Models Learn Chemistry? *J. Chem. Phys.* **2022**, *156*.

(66) Hirshfeld, F. L. Bonded-Atom Fragments for Describing Molecular Charge Densities. *Theor. Chem. Acc.* **1977**, *44*, 129–138.

(67) Marenich, A. V.; Jerome, S. V.; Cramer, C. J.; Truhlar, D. G. Charge Model 5: An Extension of Hirshfeld Population Analysis for the Accurate Description of Molecular

Interactions in Gaseous and Condensed Phases. *J. Chem. Theory Comput.* **2012**, *8*, 527–541.

(68) Kubecka, J.; Besel, V.; Kurtén, T.; Myllys, N.; Vehkamaki, H. Configurational Sampling of Noncovalent (Atmospheric) Molecular Clusters: Sulfuric Acid and Guanidine. *J. Phys. Chem. A* **2019**, *123*, 6022–6033.

(69) Grimme, S. Supramolecular Binding Thermodynamics by Dispersion-Corrected Density Functional Theory. *Chem. Eur. J.* **2012**, *18*, 9955–9964.

(70) Luchini, G.; Alegre-Requena, J. V.; Funes-Ardoiz, I.; Paton, R. S. GoodVibes: Automated Thermochemistry for Heterogeneous Computational Chemistry Data. *F1000Research* **2020**, *9*, 291.

(71) Riplinger, C.; Neese, F. An Efficient and Near Linear Scaling Pair Natural Orbital Based Local Coupled Cluster Method. *J. Chem. Phys.* **2013**, *138*.

(72) Riplinger, C.; Sandhoefer, B.; Hansen, A.; Neese, F. Natural Triple Excitations in Local Coupled Cluster Calculations with Pair Natural Orbitals. *J. Chem. Phys.* **2013**, *139*.

(73) Dennington, A.; Keith, T. A.; Millam, J. M. GaussView Version 6. 2019; Semichem Inc. Shawnee Mission KS.

(74) Dzidic, I.; Kebarle, P. Hydration of the Alkali Ions in the Gas Phase. Enthalpies and Entropies of Reactions $M^+(H_2O)_{n-1} + H_2O = M^+(H_2O)_n$. *J. Phys. Chem.* **1970**, *74*, 1466–1474.

(75) Schulz, C. P.; Haugstätter, R.; Tittes, H. U.; Hertel, I. V. Free Sodium-Water Clusters. *Phys. Rev. Lett.* **1986**, *57*, 1703.

(76) Schulz, C. P.; Haugstätter, R.; Tittes, H. U.; Hertel, I. V. Free Sodium-Water Clusters:

Photoionisation Studies in a Pulsed Molecular Beam Source. *Z. Phys. D* **1988**, *10*, 279–290.

(77) Hertel, I. V.; Hüglin, C.; Nitsch, C.; Schulz, C. P. Photoionization of $Na(NH_3)_n$ and $Na(H_2O)_n$ Clusters: A Step Towards the Liquid Phase? *Phys. Rev. Lett.* **1991**, *67*, 1767.

(78) Patwari, G. N.; Lisy, J. M. Mimicking the Solvation of Aqueous Na^+ in the Gas Phase. *J. Chem. Phys.* **2003**, *118*, 8555–8558.

(79) Vaden, T. D.; Weinheimer, C. J.; Lisy, J. M. Evaporatively Cooled $M^+(H_2O)Ar$ Cluster Ions: Infrared Spectroscopy and Internal Energy Simulations. *J. Chem. Phys.* **2004**, *121*, 3102–3107.

(80) Mancinelli, R.; Botti, A.; Bruni, F.; Ricci, M. A.; Soper, A. K. Hydration of Sodium, Potassium, and Chloride Ions in Solution and the Concept of Structure Maker/Breaker. *J. Phys. Chem. B* **2007**, *111*, 13570–13577.

(81) Perez, P.; Lee, W. K.; Prohofsky, E. W. Study of Hydration of the Na^+ Ion Using a Polarizable Water Model. *J. Chem. Phys.* **1983**, *79*, 388–392.

(82) Arbman, M.; Siegbahn, H.; Pettersson, L.; Siegbahn, P. Core Electron Binding Energies and Auger Electron Energies of Solvated Clusters: A Computational Study. *Mol. Phys.* **1985**, *54*, 1149–1160.

(83) Lybrand, T. P.; Kollman, P. A. Water–Water and Water–Ion Potential Functions Including Terms for Many Body Effects. *J. Chem. Phys.* **1985**, *83*, 2923–2933.

(84) Cieplak, P.; Lybrand, T. P.; Kollman, P. A. Calculation of Free Energy Changes in Ion–Water Clusters Using Nonadditive Potentials and the Monte Carlo Method. *J. Chem. Phys.* **1987**, *86*, 6393–6403.

(85) Probst, M. M. A Study of the Additivity of Interactions in Cation-Water Systems. *Chem. Phys. Lett.* **1987**, *137*, 229–232.

(86) Bauschlicher Jr., C. W.; Langhoff, S. R.; Partridge, H.; Rice, J. E.; Komornicki, A. A Theoretical Study of $Na(H_2O)_n^+$ (n= 1–4). *J. Chem. Phys.* **1991**, *95*, 5142–5148.

(87) Dang, L. X.; Rice, J. E.; Caldwell, J.; Kollman, P. A. Ion Solvation in Polarizable Water: Molecular Dynamics Simulations. *J. Am. Chem. Soc.* **1991**, *113*, 2481–2486.

(88) Perera, L.; Berkowitz, M. L. Many-Body Effects in Molecular Dynamics Simulations of $Na^+(H_2O)_n$ and $Cl^-(H_2O)_n$ Clusters. *J. Chem. Phys.* **1991**, *95*, 1954–1963.

(89) Hashimoto, K.; Morokuma, K. Ab Initio Molecular Orbital Study of $Na(H_2O)_n$ (n = 1–6) Clusters and Their Ions. Comparison of Electronic Structure of the" Surface" and" Interior" Complexes. *J. Am. Chem. Soc.* **1994**, *116*, 11436–11443.

(90) Glendening, E. D.; Feller, D. Cation–Water Interactions: The $M^+(H_2O)_n$ Clusters for Alkali Metals, M = Li, Na, K, Rb, and Cs. *J. Phys. Chem.* **1995**, *99*, 3060–3067.

(91) Kim, J.; Lee, S.; Cho, S. J.; Mhin, B. J.; Kim, K. S. Structures, Energetics, and Spectra of Aqua-Sodium (I): Thermodynamic Effects and Nonadditive Interactions. *J. Chem. Phys.* **1995**, *102*, 839–849.

(92) Ramaniah, L. M.; Bernasconi, M.; Parrinello, M. Density-Functional Study of Hydration of Sodium in Water Clusters. *J. Chem. Phys.* **1998**, *109*, 6839–6843.

(93) Carrillo-Tripp, M.; Saint-Martin, H.; Ortega-Blake, I. A Comparative Study of the Hydration of Na^+ and K^+ with Refined Polarizable Model Potentials. *J. Chem. Phys.* **2003**, *118*, 7062–7073.

(94) Lee, H. M.; Tarakeshwar, P.; Park, J.; Kołaski, M. R.; Yoon, Y. J.; Yi, H.-B.; Kim, W. Y.; Kim, K. S. Insights into the Structures, Energetics, and Vibrations of Monovalent Cation–$(Water)_{1-6}$ Clusters. *J. Phys. Chem. A* **2004**, *108*, 2949–2958.

(95) Rao, J. S.; Dinadayalane, T. C.; Leszczynski, J.; Sastry, G. N. Comprehensive Study on the Solvation of Mono- and Divalent Metal Cations: Li^+, Na^+, K^+, Be^{2+}, Mg^{2+} and Ca^{2+}. *J. Phys. Chem. A* **2008**, *112*, 12944–12953.

(96) Neela, Y. I.; Mahadevi, A. S.; Sastry, G. N. First Principles Study and Database Analyses of Structural Preferences for Sodium Ion (Na^+) Solvation and Coordination. *Struct. Chem.* **2013**, *24*, 67–79.

(97) Biring, S. K.; Sharma, R.; Misra, R.; Chaudhury, P. Structural and Infra Red Spectroscopic Aspects of Ion-Water Clusters: A Study Based on a Combined Stochastic and Quantum Chemical Approach. *J. Clust. Sci.* **2013**, *24*, 715–737.

(98) Dinh, P. M.; Gao, C. Z.; Klüpfel, P.; Reinhard, P.-G.; Suraud, E.; Vincendon, M.; Wang, J.; Zhang, F. S. A Density Functional Theory Study of $Na(H_2O)_n$: An Example of the Impact of Self-Interaction Corrections. *Eur. Phys. J. D* **2014**, *68*, 1–8.

(99) Soniat, M.; Rogers, D. M.; Rempe, S. B. Dispersion- and Exchange-Corrected Density Functional Theory for Sodium Ion Hydration. *J. Chem. Theory Comput.* **2015**, *11*, 2958–2967.

(100) Fifen, J. J.; Agmon, N. Structure and Spectroscopy of Hydrated Sodium Ions at Different Temperatures and the Cluster Stability Rules. *J. Chem. Theory Comput.* **2016**, *12*, 1656–1673.

(101) Wang, P.; Shi, R.; Su, Y.; Tang, L.; Huang, X.; Zhao, J. Hydrated Sodium Ion Clusters $[Na^+(H_2O)_n$ (n = 1–6)]: An Ab Initio Study on Structures and Non-Covalent Interaction. *Front. Chem.* **2019**, *7*, 624.

(102) Keesee, R. G.; Castleman Jr, A. W. Gas-Phase Studies of Hydration Complexes of Cl^- and I^- and Comparison to Electrostatic Calculations in the Gas Phase. *Chem. Phys. Lett.* **1980**, *74*, 139–142.

(103) Likholyot, A.; Hovey, J. K.; Seward, T. M. Experimental and Theoretical Study of Hydration of Halide Ions. *Geochim. Cosmochim. Acta* **2005**, *69*, 2949–2958.

(104) Xantheas, S. S. Quantitative Description of Hydrogen Bonding in Chloride–Water Clusters. *J. Phys. Chem.* **1996**, *100*, 9703–9713.

(105) Masamura, M. Structures, Energetics, and Spectra of $Cl^-(H_2O)_n$ Clusters, n = 1–6: Ab Initio Study. *J. Phys. Chem. A* **2002**, *106*, 8925–8932.

(106) Xantheas, S. S.; Dunning Jr, T. H. Ab Initio Studies of Cyclic Water Clusters $(H_2O)_n$, n = 1–6. I. Optimal Structures and Vibrational Spectra. *J. Chem. Phys.* **1993**, *99*, 8774–8792.

(107) Xantheas, S. S. Ab Initio Studies of Cyclic Water Clusters $(H_2O)_n$, n = 1–6. II. Analysis of Many-Body Interactions. *J. Chem. Phys.* **1994**, *100*, 7523–7534.

(108) Xantheas, S. S. Ab Initio Studies of Cyclic Water Clusters $(H_2O)_n$, n = 1–6. III. Comparison of Density Functional with MP2 Results. *J. Chem. Phys.* **1995**, *102*, 4505–4517.

(109) Shemesh, D.; Luo, M.; Grassian, V. H.; Gerber, R. B. Absorption Spectra of Pyruvic Acid in Water: Insights from Calculations for Small Hydrates and Comparison to Experiment. *Phys. Chem. Chem. Phys.* **2020**, *22*, 12658–12670.

(110) Li, S.; Kjaergaard, H. G.; Du, L. Infrared Spectroscopic Probing of Dimethylamine Clusters in an Ar Matrix. *J. Environ. Sci.* **2016**, *40*, 51–59.

(111) Du, L.; Mackeprang, K.; Kjaergaard, H. G. Fundamental and Overtone Vibrational Spectroscopy, Enthalpy of Hydrogen Bond Formation and Equilibrium Constant Determination of the Methanol–Dimethylamine Complex. *Phys. Chem. Chem. Phys.* **2013**, *15*, 10194–10206.